Article

Interaction of Hydrocarbons with Clays at Reservoir Conditions: in situ IR and NMR Spectroscopy and X-ray Diffraction for Expandable Clays with Variably Wet Supercritical Methane

Geoffrey M Bowers, John S. Loring, Herbert Todd Schaef, Eric D. Walter, Sarah D Burton, David W. Hoyt, Sydney S. Cunniff, Narasimhan Loganathan, and R. James Kirkpatrick

ACS Earth Space Chem., **Just Accepted Manuscript** • DOI: 10.1021/acsearthspacechem.8b00039 • Publication Date (Web): 07 May 2018

Interaction of Hydrocarbons with Clays at Reservoir Conditions: *in situ* IR and NMR Spectroscopy and X-ray Diffraction for Expandable Clays with Variably Wet Supercritical Methane

Geoffrey M. Bowers[1], John S. Loring[2*], H. Todd Schaef [2], Eric D. Walter[3], Sarah D. Burton[3], David W. Hoyt[3], Sydney S. Cunniff[1], Narasimhan Loganathan[4], R. James Kirkpatrick[5]*

[1]Department of Chemistry and Biochemistry, St. Mary's College of Maryland, St. Mary's City, MD 20686

[2]Physical and Computational Sciences Directorate, Pacific Northwest National Laboratory, Richland, WA, 99352

[3]William R. Wiley Environmental and Molecular Sciences Laboratory, Pacific Northwest National Laboratory, Richland, WA, 99352

[4]Department of Chemistry, Michigan State University, East Lansing, MI, 48824

[5]Departments of Chemistry and Earth and Environmental Sciences, Michigan State University, East Lansing, MI, 48824

*Corresponding Author Info: gmbowers1@smcm.edu - Geoffrey Bowers; john.loring@pnl.gov - John Loring

ABSTRACT

The results from a novel *in situ* high-pressure nuclear magnetic resonance (NMR) spectroscopy, infrared (IR) spectroscopy, and X-ray diffraction (XRD) investigation of the interaction of the smectite hectorite with variably wet supercritical methane ($scCH_4$) at 90 bar and 323 K (hydrostatic conditions equivalent to ~ 1 km depth) show that CH_4 occurs in the clay interlayers, in pores external to the individual clay particles, and as bulk fluid. The occupancy of each environment depends on the relative humidity (RH) of the CH_4-rich fluid and the hydration energy and size of the charge-balancing cation. As RH increases, the fraction of interlayer and inter-particle CH_4 decreases, although with Cs^+, addition of a small amount of H_2O initially increases CH_4 uptake. Maximum interlayer CH_4 adsorption occurs when the mean basal spacing just permits methane intercalation (~11.5 Å) and never below this basal spacing. It is also higher with divalent cations than with monovalent cations. The data show that CH_4 adsorption occurs predominantly via a weak, dispersion interaction with the clay and that its intercalation occurs via a passive, space-filling hydrophobic mechanism. The results suggest that under reservoir conditions smectite interlayers may provide a reservoir for CH_4 under low-water conditions.

KEYWORDS: shale gas, tight gas, methane, hydrofracking, carbon capture and utilization, smectite

INTRODUCTION

Recent developments in hydraulic fracturing technologies have resulted in greatly increased natural gas production from shale and other tight gas reservoirs. Based on current trends, the extractable gas from these types of formations is projected to provide over 100 trillion cubic feet (Tcf) of new gas in North America alone, which is enough for several decades of U.S. demand.[1] Worldwide, estimates suggest that these unconventional gas resources can be as large as the conventional resource pool.[2] There are, however, many concerns associated with current shale gas extraction technologies (hydrofracking), including the environmental impacts from the chemicals used, heavy metal and other contamination in flowback water, the intensive use of water, and physical damage to the rock formation that can affect the subsurface hydrology.[3-4] Therefore, it is prudent to consider alternatives to conventional fracking fluids that minimize these undesirable environmental impacts, particularly if alternative fluids convert a waste stream into a value-added commercial product (e.g. CO_2). Efficient selection and/or design of such alternatives requires detailed understanding of CH_4 binding and dynamics in shales and relevant model materials on the molecular scale. Unfortunately, molecular scale studies of these complex, heterogeneous materials under reservoir pressures and temperatures remain challenging.[5]

Previous experimental thermodynamic studies of CH_4/shale interaction have suggested that the smectitic components of the clay mineral fraction (swelling clays and the smectite layers of mixed illite/smectite) play an important role in CH_4 adsorption. X-ray diffraction (XRD) and adsorption isotherm measurements by Liu et al. show that Ca-montmorillonite adsorbs significantly more CH_4 than illite or kaolinite at 333 K and pressures up to 180 bar.[6] Their results also suggest that CH_4 and H_2O compete for adsorption sites, that signifcant H_2O adsorption prevents the adsorption of CH_4 by phyllosilicates, and that CH_4 can be adsorbed in the interlayers

of Ca-montmorillonite. Due to the large hydration energy of Ca^{2+}, smectite interlayers containing Ca are difficult to dehydrate, and several features of their data suggest that the CH_4 may be adsorbed in inter-particle pores and on external surface sites rather than in the interlayer galleries. For example, the increased CH_4 adsorption capacity of the sample heated to 200°C is likely all due to external surface sites, since the corresponding XRD pattern shows fully hydrated 2WL-type interlayers that should prevent significant CH_4 intercalation. Several studies have shown that the CH_4 adsorption capacities of smectites and clay-rich shales correlate with the pore structure and pore surface area.[7-9] For instance, Ji et al. showed that the CH_4 adsorption capacity of montmorillonites and mixed illite-smectites correlate with the micro- and meso-porosity in the nm to tens of nm pore size range.[8] They also report heats of adsorption (q) and entropies of adsorption (ΔS) for CH_4 adsorbed to montmorillonite, mixed-layer illite-smectite, kaolinite, chlorite, and illite between q = 9.4 and 16.6 kJ mol^{-1} and ΔS = -64.8 to -79.5 J mol^{-1} K^{-1}. These values are much lower than for CH_4 adsorption by the organic material (kerogen) commonly found in shale. However, shales typically contain much larger amounts of smectitic minerals than kerogen, and CH_4 adsorption on the clay components may dominate in shale types that are rich in clay. In addition, experimental isosteric heats of adsorption for CH_4 on montmorillonite, kaolinite, illite, and chlorite show that the interactions of CH_4 with smectites are stronger than for other phyllosilicate phases.[7] Thus, smectites are likely to play an important role in CH_4/rock interactions in clay-rich rocks such as shales, and the presence of H_2O is likely to have a significant effect on CH_4 adsorption and dynamics. The available experimental data are, however, less clear regarding the specific types of sites available for CH_4 adsorption (for example, whether CH_4 can intercalate smectitic interlayers or not) and how their occupancy

evolves with the thermodynamic water activity and other factors. This is due largely to a lack of molecular-scale data.

Much of what is known about CH_4-smectite interactions on a molecular scale comes from computational molecular modeling using principally Grand Canonical Monte Carlo (GCMC) methods. Rao and colleagues used a combination of GCMC and molecular dynamics (MD) methods to examine Na-montmorillonite at 300 K and pressures from 20-50 bar in contact with wet methane and mixtures of methane, water, and other small hydrocarbons such as ethane.[10-11] They found that initial swelling of the smectite occurs via H_2O adsorption and that CH_4 can intercalate the interlayers after they have expanded to basal spacings of at least ~12.5 Å (a monolayer hydrate). Despite the observation of interlayer CH_4 in hydrated and expanded interlayers with basal spacings up to 24 Å, the results indicate that high relative humidity (RH) can inhibit CH_4 intercalation in montmorillonites. This conclusion is in good agreement with the adsorption isotherm results of Liu[6] discussed above. Rao et al. also report that CH_4 molecules form clusters within the hydrated interlayers largely because of their hydrophobicity. Such water-avoidance clustering has also been suggested for interlayer CO_2 in montmorillonite at supercritical conditions relevant to the shallow subsurface.[12] Zhang and Cao used GCMC calculations to examine displacement of CH_4 by CO_2 in clay-organic composites at conditions relevant to reservoirs at 1-4 km depth.[13] They find that the total displacement of CH_4 is linked closely to the pore sizes in the system, consistent with the adsorption isotherm studies.[6-9] Likewise, these GCMC results suggest that CH_4 and CO_2 both spontaneously adsorb to the external surfaces of illite and that CH_4 adsorption is generally dominated by CH_4-surface interactions rather than CH_4-cation interactions.[14] This later result is consistent with the idea that cation-rich smectite interlayers may be less favorable CH_4 binding environments than external

smectite surfaces, a manifestation of the well-known "salting out effect" where salt in aqueous systems reduces the solubility of gases. Such an effect has been observed for CH_4 interactions in clay nano-pores in simulations and gravimetric measurements by Gadikota et al.[15] Adsorption of CH_4, predominantly in monolayers on external surfaces, was observed at room temperature and several different CH_4 pressures in simulations by Jin and Firoozabadi,[16] who suggest that dispersive interactions are responsible for CH_4-smectite interaction and that CH_4 adsorption is mainly a function of the smectite surface area. A recent ab initio molecular dynamics (AIMD) study by Lee and colleagues examined the interaction of $H_2O/CH_4/CO_2$ fluids with Ca-montmorillonite at pressures between 0 and 120 bar CH_4.[17] Their model suggests a basal expansion of ~10% for smectite with 2-5 H_2O/Ca^{2+} upon intercalation of CH_4, that adsorption of CH_4 produces relatively large dipole moments in the methane molecules, and that the clay surfaces prefer CO_2 and H_2O to CH_4. They also report larger basal expansions with CH_4 intercalation than with the intercalation of CO_2 at 4 H_2O/cation and that polar CH_4 can dehydrate interlayer cations. Overall, the computational studies suggest that the RH and pore surface area are the most significant controls of CH_4-smectite interactions. These conclusions are largely consistent with the adsorption isotherm studies that show CH_4-smectite interactions are dominated by weak hydrophobic-type forces and that CH_4 can intercalate into the interlayer galleries of smectites only under specific conditions.

Spectroscopic studies providing molecular-scale details of CH_4/mineral interactions at elevated temperatures and pressures relevant to the subsurface are very limited[18-19] but are needed to validate the computational predictions and provide a molecular foundation for interpreting the adsorption isotherm results. Ok et al. recently used a combination of computational molecular modeling and ^{13}C magic angle spinning (MAS) nuclear magnetic resonance (NMR) spectroscopy

to show that the ^{13}C chemical shift of CH_4 is sensitive to the pore structure of mesoporous silica.[19] For bulk CH_4 they observe a change in the peak position to less negative (less shielded) chemical shifts with increasing CH_4 pressure between 28 and 130 bar at 35°C and 73°C. They attribute the development of a second resonance at ~0.6 ppm less negative chemical shifts to methane in 4 nm nano-pores and its densification against the pore walls. Although not at elevated temperature, NMR studies of $^{13}CH_4$ in the pores in molecular sieves, in hydrate phases, and in methane hydrates formed in smectite interlayers also have less shielded ^{13}C chemical shifts.[20-26] We are aware of no such spectroscopic studies of smectite/CH_4 systems at elevated temperature and pressure. Clearly, more experimental data at conditions relevant to natural gas and C-sequestration reservoirs are needed to provide additional insight into CH_4/smectite interactions and how the fluid and smectite properties influence these interactions.

This paper describes *in situ,* experimental infrared (IR) and NMR spectroscopy and X-ray diffraction (XRD) results for the smectite mineral hectorite in contact with variably wet supercritical methane ($scCH_4$) at 323 K and 90 bar CH_4. These conditions are equivalent to ~ 1 km depth in the earth and have been previously used for study of CO_2-smectite interactions relevant to subsurface reservoirs.[27-34] The results provide novel insight into the molecular scale behavior of CH_4/smectite binding and show that CH_4 can adsorb in both the interlayer galleries and in larger external pores between clay particles. Fluid RH and the properties of the charge balancing cation (e.g., hydration energy and size) play important roles in the CH_4 behavior. The data are consistent with CH_4 adsorption in smectites being driven largely by hydrophobic interactions rather than electrostatic forces and with intercalation occurring via a passive, space-filling mechanism when the basal spacings are ~11.5 Å or larger. These conclusions are in excellent agreement with the published adsorption isotherm and molecular modeling results

discussed above. Since CH_4 adsorption is driven by a hydrophobic mechanism, more hydrophobic smectites, such as those containing significant quantities of fluorine[35], are likely to better sorb methane than smectites with greater hydrophilicity.

MATERIALS AND EXPERIMENTAL METHODS

The smectite used here is the natural San Bernardino hectorite (SHCa-1) available from the Source Clays Repository of the Clay Mineral Society (CMS). Like montmorillonite, hectorite develops its negative layer charge by dominantly substitution in the octahedral layer and is preferable for high resolution NMR studies due to its low structural Fe content that minimizes paramagnetic effects on the NMR spectra. We used the < 1 μm fraction isolated via differential centrifugation and freed of carbonate via the acetic acid titration approach of Arroyo et al.[36] XRD and thermogravimetric analysis (TGA) shows that this sample fraction contains a small amount of quartz and Ca-carbonate that survived the purification process; typically < 0.5% of the sample by weight. Ion exchange procedures to produce the Ca-, Cs-, and Na-hectorites followed those used previously by our group; these and the Pb-hectorite exchange procedures are described in the Supplemental Materials.[27, 37-38]

Samples were characterized at 323 K and 90 bar CH_4 pressure using a suite of novel high pressure instruments at Pacific Northwest National Laboratory. *In situ* transmission and attenuated total reflection (ATR) IR spectra were acquired for the cation-exchanged hectorites using a fully automated supercritical fluid generation and delivery apparatus coupled to a high-pressure IR cell.[39] After exposure of the samples to vacuum conditions at 323 K for at least 30 minutes, $scCH_4$ was introduced and the spectra were acquired as the RH of the $scCH_4$ was progressively increased from 0% to ~85%. The transmission spectra were analyzed to determine

the RH values and amount of H_2O adsorbed at each RH. The amount of H_2O adsorbed by the sample at each step in the titration is the difference between the H_2O added to the high pressure IR cell and the H_2O content of the vapor phase. The ATR IR data were used to characterize the adsorbed CH_4 at each RH. Detailed descriptions of the apparatus, high pressure cell, and the experimental methods for performing these titrations are reported by Thompson et al.[39], Loring et al.[28], and Bowers et al.[27] *In situ* XRD patterns were collected for the hectorite samples at 323 K and 90 bar fluid pressure using a high pressure and temperature X-ray diffraction instrument[30, 40-41] coupled to an IR spectrometer with a high pressure transmission gas cell.[42-43] Both components were fitted to a supercritical fluid manipulation system. The diffraction patterns were collected first under vacuum and then with increasing RH of the $scCH_4$ between 0% and 100%. *In situ* ^{13}C MAS NMR spectra were acquired for the cation-exchanged hectorites at 323 K and 90 bar CH_4 pressure using a home-built 5 mm double resonance probe and an 11.7 T Agilent VNMRS console at the William R. Wiley Environmental and Molecular Sciences Laboratory at Pacific Northwest National Laboratory. A 100% ^{13}C-enriched CH_4 fluid was introduced into the NMR rotor containing the sample using the WHiMS flow system[44] we have employed previously.[27] To control the H_2O content, samples were either dried in a vacuum oven at 323 K for 12-24 hours or exposed overnight to a saturated $K_2CO_3/^2H_2O$ solution (43% RH) or over bulk ^2H_2O (100% RH) at room temperature before being rapidly sealed in the rotor. Note that these RH values do not correspond to the actual humidity in the NMR rotors during data acquisition because the dry $scCH_4$ will extract some ^2H_2O from the clays and the NMR experiments are conducted at a temperature above the equilibration temperature. All discussion of the variably hydrated NMR samples and NMR results refer to the initial RH of equilibration at atmospheric T and P before exposure to dry supercritical CH_4.

RESULTS

H_2O Adsorption by Hectorite at 90 bar CH_4 and 323 K

The transmission IR spectra of the four cation exchanged hectorites from the $scCH_4$ RH-titrations (Figure 1) show that the amount of adsorbed H_2O increases with increasing RH, paralleling the previously observed behavior of hectorite and montmorillonites with $scCO_2$ under the same conditions.[27-28, 30] The Pb- and Ca-hectorites adsorb more H_2O than the Na- and Cs-hectorites, consistent with the hydration behavior of smectite clays under ambient conditions, the known correlation between the extent of hectorite hydration at a given RH and the hydration energy of the charge balancing cation (E_{hyd} Ca^{2+} > Pb^{2+} >> Na^+ > Cs^+)[37-38, 45-46], and the reduced number of interlayer cations since Pb^{2+} and Ca^{2+} are both divalent and only half the ions are needed to balance the layer charge.[15] Importantly, the Pb- and Ca-hectorites contain substantial amounts of H_2O after equilibration under vacuum and adsorb more H_2O at a given RH than the Cs- and Na-hectorites consistent with the behavior of hectorite with $scCO_2$ at this temperature and pressure.[27] Although there is detectable adsorbed H_2O for the Na- and Cs-hectorites under vacuum conditions, the amount is much less than for Pb- and Ca-hectorite.

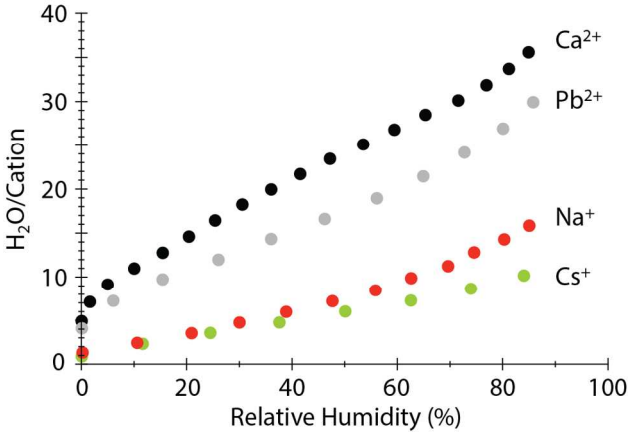

Figure 1. Water uptake by the hectorites with the indicated exchangeable cations as a function of the RH of the $scCH_4$ obtained from the IR titration vapor phase transmission data expressed as H_2O/cation mole ratio. For the same plot expressed as mmol H_2O/g clay as a function of RH, see Supporting Information Figure S1.

The XRD results also show that the samples expand with increasing RH according to the trends expected based on the cation hydration energies (Figure 2).[37-38, 47-48] With increasing RH, Cs-hectorite expands to a basal spacing of ~12.2 Å at ~40% RH in an essentially step-wise fashion and remains at this spacing up to 100% RH. This basal spacing is similar to that of smectites containing a monolayer of adsorbed H_2O in its interlayers, which will be referred to as 1WL-type interlayers in the remainder of this paper. For Na-hectorite under vacuum, the skewed basal reflection shows the presence of principally collapsed interlayers (0WL-type) with some 1WL-type interlayers, consistent with the presence of some residual water molecules, as shown in the transmission IR results above. Na-hectorite begins to expand at ~30- 40% RH, and with increasing RH it develops a broader basal peak that increases in intensity. The large breadth of this peak indicates heterogeneous expansion[28, 30] with a mixture of 0WL-type, 1WL-type, and 2WL-type

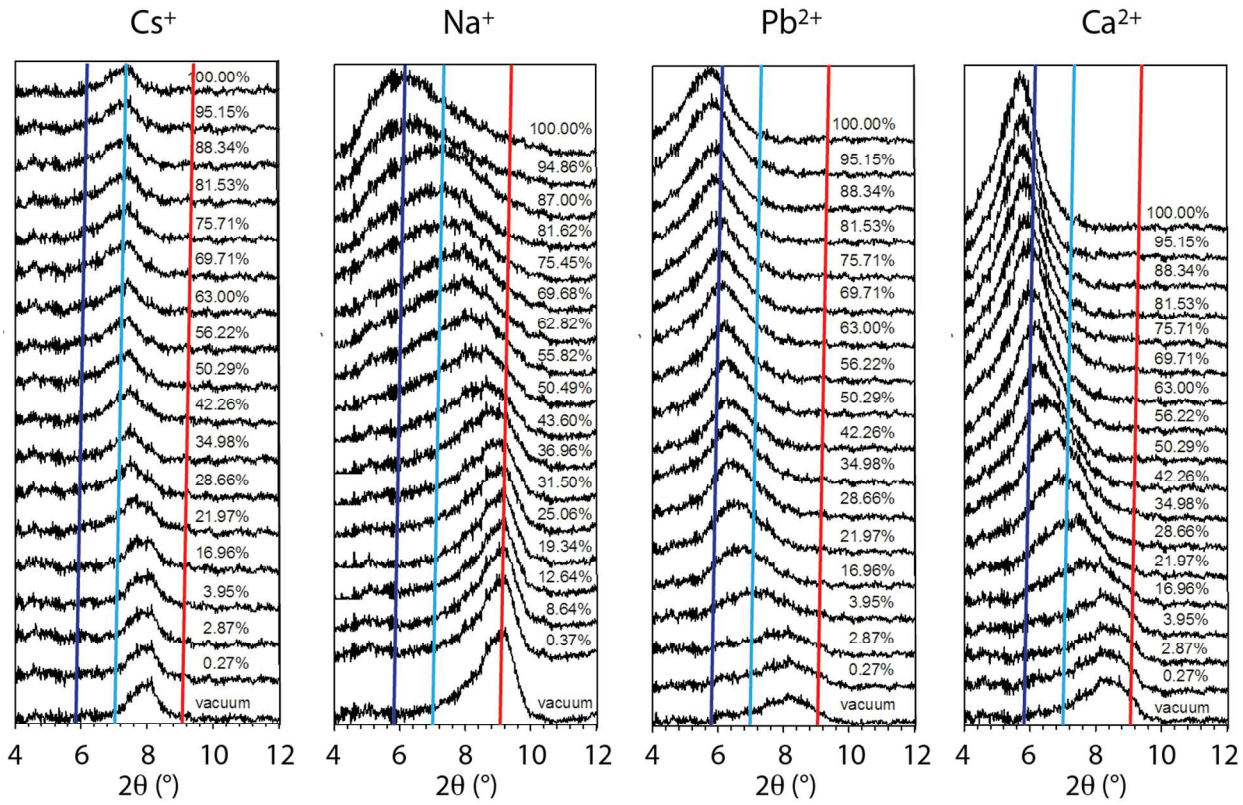

Figure 2. *In situ* XRD patterns for the indicated ion-exchanged hectorite samples with the indicated RH of the $scCH_4$ phase. The data are presented from left-to-right as a function of increasing hydration energy of the charge-balancing cation. The vertical lines mark the typical positions of reflections associated with collapsed (9.8 Å; red), 1WL-type (12.5 Å; light blue), and 2WL-type (15 Å; dark blue) interlayers. Over the humidity range investigated here, the Cs-hectorite basal spacing starts at 11.2 Å and maxes out at 12.2 Å; Na-hectorite ranges from 9.8 Å to 15.0 Å; Pb-hectorite from 10.8 Å to 16.0 Å; and Ca-hectorite from 10.6 Å to 16.1 Å. The results show how both the Na- and Cs-hectorites have a significant number of 1WL-type interlayers at 100% RH in $scCH_4$ at 90 bar and 323 K. The diffraction patterns were collected first under vacuum and then with increasing RH of the $scCH_4$ from a very low value (0.27 or 0.37%) to 100%.

(interlayers with basal spacings of ~15 Å) structures even at 100% RH. The high RH for the onset of expansion contrasts with the data for Na-hectorite at atmospheric pressure and temperature, which show expansion at relatively low RHs.[37] This difference may indicate either slower hydration kinetics at elevated T and P or that $scCH_4$ at these conditions provides a barrier to interlayer hydration (clogging of interlayer pore throats, for example). Under vacuum and low RH conditions the basal reflections of the Pb- and Ca-hectorites are relatively broad and indicate

the presence of a mixture of 0WL-type and 1WL-type interlayers with more 1WL-type layers, consistent with the presence of significant amounts of H_2O at low RH observed in the transmission IR data above. These samples expand continuously with increasing RH and are dominated by 2WL-type interlayers at high RHs. This behavior parallels the previously observed behavior of Ca-hectorite in contact with variably wet $scCO_2$ at 90 bar and 323 K[27] and also at room temperature and pressure[38], although the basal spacings are larger at all RH values at atmospheric temperature and pressure. The 2WL-type structure is expected over much of the RH range if the interlayer expansion is dominated by cation hydration, due to the high hydration energies of the divalent cations (1481 kJ/mol and 1577 kJ/mol, for Pb^{2+} and Ca^{2+}, respectively[46]).

CH_4 Adsorption by Vacuum Dried Hectorite

The *in situ* high pressure XRD results show that exposure to dry $scCH_4$ does not cause significant interlayer expansion for any of the samples examined here (Figures 2 and S2). The basal spacings under vacuum and in contact with dry $scCH_4$ are 11.2 Å vs. 11.1 Å for Cs-hectorite, 9.8 Å vs. 9.8Å for Na-hectorite, 10.8 Å vs. 11.1 Å for Pb-hectorite, and 10.6 Å vs. 10.8 Å for Ca-hectorite. These changes are significantly less than the 10% expansion proposed based on computational modeling results for Ca-montmorillonite of Lee et al.[17] and are important for interpreting the adsorption environments for CH_4 in the vacuum-dried samples.

The ATR-IR spectra of the four cation exchanged hectorites exposed to dry $scCH_4$ contain bands for CH_4 adsorbed to the hectorite with both undistorted tetrahedral symmetry and asymmetric, non-tetrahedral symmetry (Figures 3 and S3). The spectra show the P-Q-R branches of the normal

CH_4 asymmetric C-H stretching vibrational mode between 2850 and 3150 cm^{-1}, including a large Q peak at 3000 cm^{-1}. There is also a band at ~2900 cm^{-1} that corresponds to the symmetry forbidden ν_1 vibrational mode of CH_4[49-50] that must be associated with non-tetrahedral CH_4.

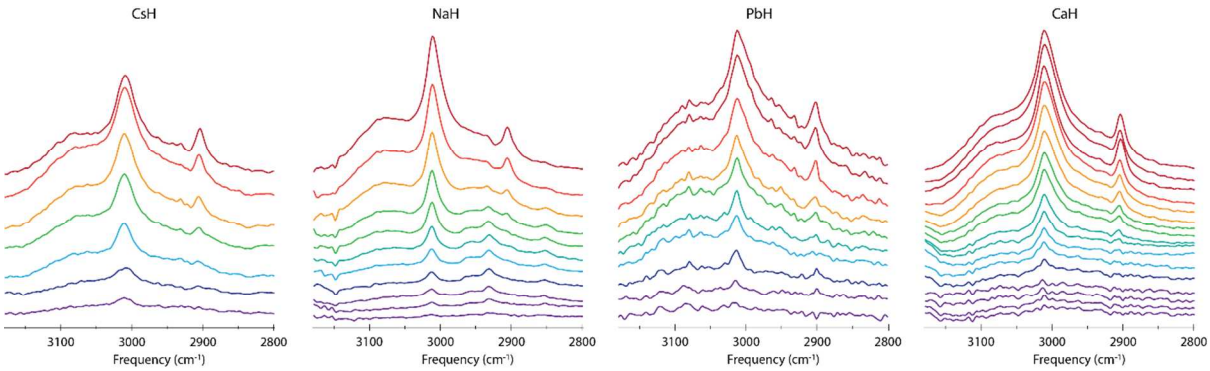

Figure 3. ATR-IR titration spectra of the four cation exchanged hectorite samples in the asymmetric stretching region for methane. Each data set is normalized to the clay O-H band and thus the intensities are comparable within each sample. The dry $scCH_4$ spectrum is at the top for each sample, and the relative humidity increases downward in each column. Each sample encountered different RHs during the titration as a result of the difference between clays in their affinity for H_2O and differences in the mass of clay present in the IR chamber. The spectra are color coded by RH: 0-10% = red, 10-20% = red/orange, 20-30% = orange, 30-40% = green, 40-50% = blue-green, 50-60% = cyan, 60-70% = dark blue, 70-85% = purple.

The ^{13}C MAS NMR spectra of the vacuum-dried hectorites exposed to dry $scCH_4$ contain several different methane resonances, with the peak positions, widths, and relative intensities dependent on the identity of the charge-balancing cation (Figures 4 and 5, Table 1). The resonance for bulk $scCH_4$ acquired in an otherwise empty rotor is similar to that published by Ok et al.[19] and consists of a very sharp peak centered at -10.3 ppm with a full-width at half-maximum (FWHH) of 0.03

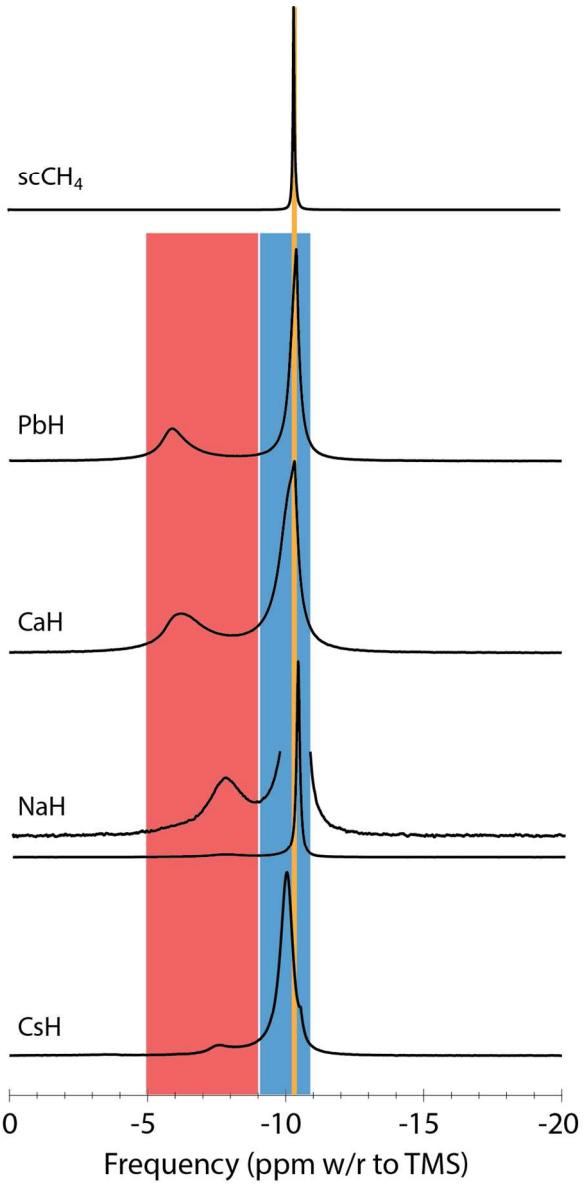

Figure 4. Comparison of the ^{1}H decoupled ^{13}C MAS NMR spectra of bulk $scCH_4$ and the various hectorite samples dried under vacuum at 50°C for 12-24 hours before being pressurized with CH_4 at 90 bar and 50°C. The red box marks the chemical shift region for the interlayer CH_4, the blue box external pore CH_4 (-10.2 ppm), and the orange line marks the position of bulk $scCH_4$.

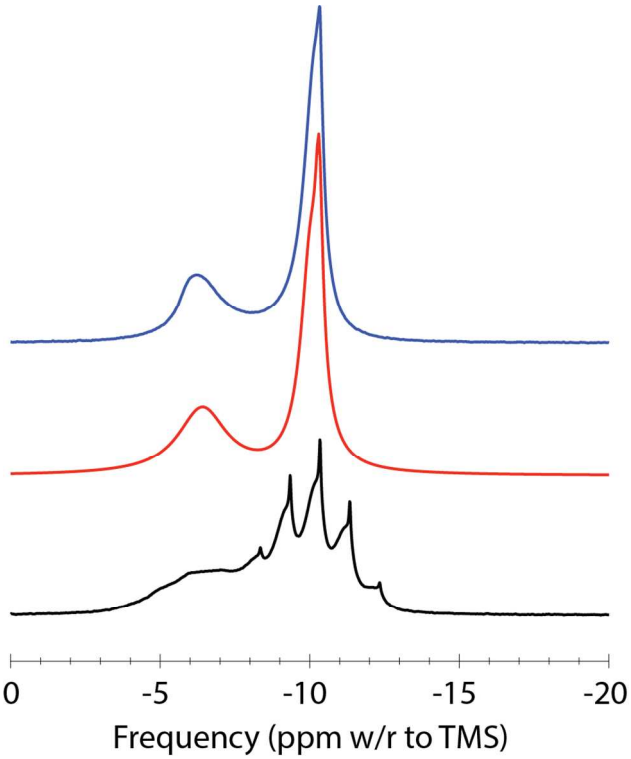

Figure 5. ^{13}C MAS NMR of vacuum dried ^{43}Ca-hectorite with ^{1}H-spinal decoupling to remove scalar and dipolar couplings (top, blue), the three site fit to the decoupled spectrum (middle, red), and without decoupling (bottom, black). The quintuplets in the un-decoupled spectrum are due to ^{1}H-^{13}C scalar (J) coupling within the methane molecules and provide greater resolution of the resonances for bulk $scCH_4$ and external pore CH_4 associated with external particle surfaces.

Table 1. ^{13}C MAS NMR chemical shifts and relative peak areas for CH_4 in hectorite at 90 bar and 323 K with the indicated exchangeable cation, designated by MH. Chemical shift values are accurate to ~ ± 0.1 ppm, peak widths to ~0.024 ppm, and relative areas to ~5%. Bulk $scCH_4$ at these conditions has an isotropic chemical shift of -10.3 ppm and a FWHH of 0.032 ppm.

		Vacuum Dried			43% RH			100% RH		
Sample	Site	δ_{iso} (ppm)	FWHH (ppm)	%Area	δ_{iso} (ppm)	FWHH (ppm)	%Area	δ_{iso} (ppm)	FWHH (ppm)	%Area
PbH	interlayer	-6.0	0.632	34%	-6.7	0.681	21%	-6.4	1.07	9%
PbH	external pore	-10.3	0.223	53%	-10.4	0.165	31%	-10.1	0.277	4%
PbH	bulk fluid	-10.4	0.076	12%	-10.4	0.092	48%	-10.4	0.100	87%
CaH	interlayer	-6.0	0.565	24%	-6.8	0.843	29%	-	-	0%
CaH	external pore	-10.2	0.350	63%	-10.2	0.247	44%	-	-	0%
CaH	bulk fluid	-10.4	0.119	12%	-10.3	0.119	27%	-10.3	0.118	100%
NaH	interlayer	-8.2	0.529	21%	-7.8	*	*	-	-	-
NaH	external pore	-10.2	0.314	53%	*	*	*	-	-	-
NaH	bulk fluid	-10.5	0.212	26%	-10.4	0.068	100%	-10.4	0.076	100%
CsH	interlayer	-7.8	0.719	10%	-6.8	0.939	10%	-6.1	1.11	5%
CsH	external pore	-10.0	0.270	89%	-10.0	0.354	89%	-	-	-
CsH	bulk fluid	-10.3	.051	<1%	-10.4	0.05	<1%	-10.3	0.110	95%

* The intensity for interlayer CH_4 in NaH at 43% RH is too low to fit with accuracy, but there is a small amount of signal for it above baseline.

The signal for external pore $scCH_4$ cannot be resolved for NaH and is not included in this table.

ppm. There is a comparably narrow resonance at the same position (± 0.1 ppm) for all the hectorite samples in $scCH_4$, demonstrating that some of the CH_4 in each sample is present in a bulk $scCH_4$ fluid. This resonance is especially well resolved as the sharp quintuplet in the spectra acquired for vacuum dried Ca-hectorite without ^1H decoupling (Figure 5). This quintuplet is due to scalar (J) coupling between the ^1H and ^{13}C of the CH_4 molecules and is eliminated in the ^1H-decoupled spectra. Koskela et al. observed a similar quintuplet for bulk CH_4 in SAPO-11.[23]

All the vacuum dried hectorite samples yield a broad peak centered between -10.0 and -10.2 ppm that overlaps significantly with the bulk CH_4 resonance (Figures 4-6; Table 1). This resonance represents CH_4 in an environment with different structural and dynamical properties than bulk $scCH_4$. Like the resonance for bulk CH_4, the undecoupled spectrum of this resonance shows the quintuplet pattern due to intramolecular ^1H-^{13}C scalar coupling.

The spectra of the vacuum dried Na-, Cs-, Ca- and Pb-hectorites contain an additional, relatively broad peak centered between -6.0 and -8.2 ppm (Figures 4 and 5; Table 1). In the undecoupled spectrum of Ca-hectorite, the -6 to -8 ppm resonance is even broader, and there are very weak maxima suggestive of the presence of scalar coupling. The poor resolution of the quintuplet peaks for this site clearly demonstrates greater dispersion of the ^{13}C chemical shifts than for the -10.0 and -10.3 ppm peak, paralleling their greater FWHHs in the decoupled spectra (Table 1). The resonances other than that of bulk CH_4 are clearly related to the presence of the clay, and we address their detailed assignment in the discussion section below.

CH_4 Adsorption by Hectorite - Variably Wet CH_4 at 90 bar and 323 K

The relative intensities and chemical shifts of the resonances associated with the clay in the ^1H-decoupled spectra change with increasing RH at which the samples were equilibrated (Figure

6, Table 1). For all of the samples, the -10.0 to -10.2 ppm resonance observed for the vacuum dried

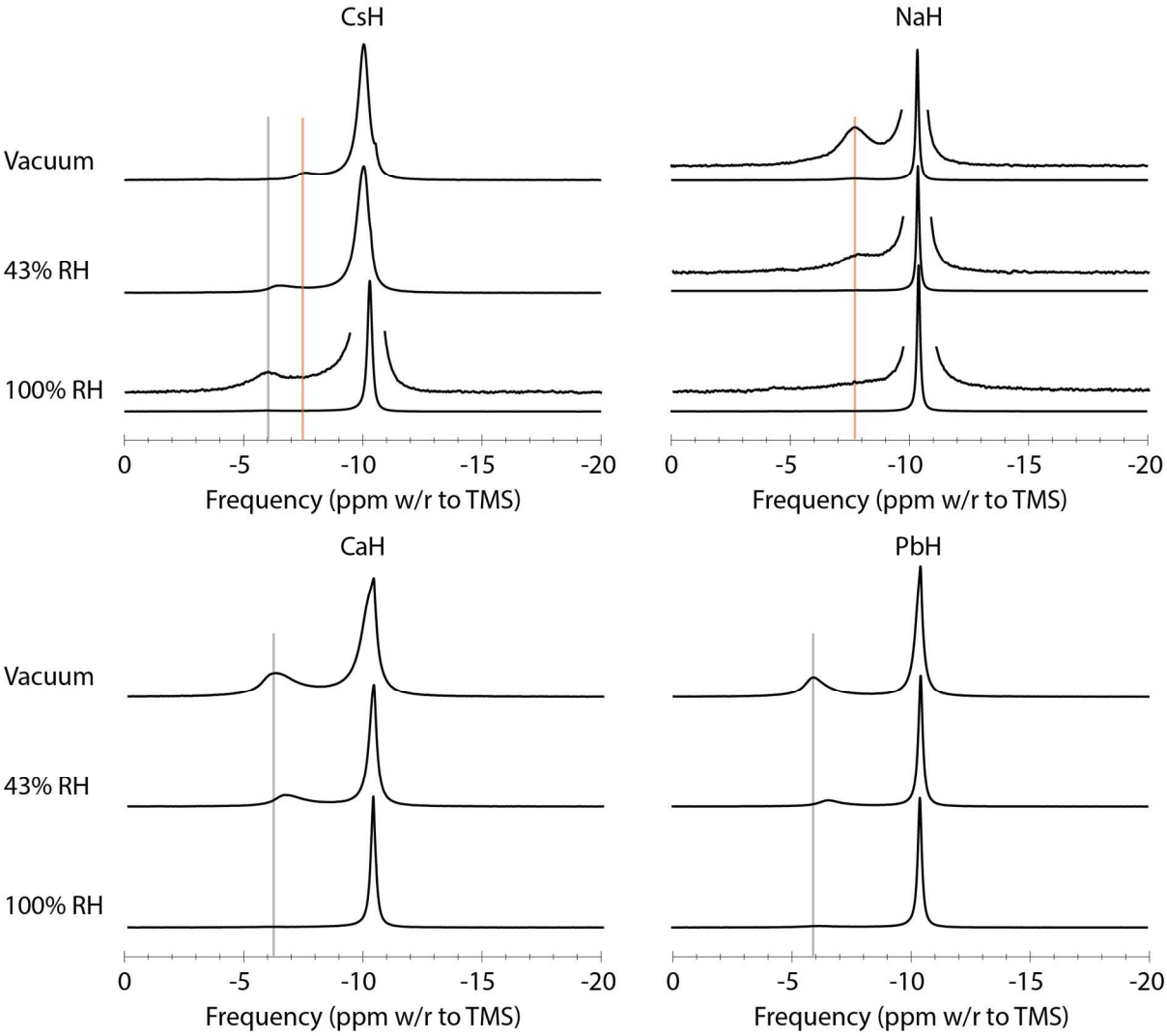

Figure 6. Comparison of the ^{1}H decoupled ^{13}C MAS NMR spectra of CH_4 in the hectorite clays used in this study. The vertical grey lines mark the Site A chemical shift region, the vertical orange lines mark the Site B chemical shift region. Here, vacuum corresponds to the sample dried under vacuum before $scCH_4$ was introduced. Recall that the %RH values correspond to the %RH at 298 K, 1 atm where the hectorite was initially equilibrated before pressurization with 90 bar CH_4 at 323 K.

samples narrows substantially at 43% RH and even more at 100% RH (Table 1). Simultaneously, its chemical shift approaches that of bulk $scCH_4$, with the two peaks merging together at 100% RH. However, some CH_4 must remain in this site at 100% RH, since the peak

widths of the merged peak are larger than for bulk CH_4 (0.1 ± 0.02 ppm vs. 0.032 ppm). For the Pb- and Ca-hectorites, the relative intensities of the -6.0 ppm resonances decrease at 43% and 100% RH, and the peak positions become slightly more negative. For Ca-hectorite, at 100% RH this resonance is not observable above baseline. For Cs-hectorite, this resonance moves from -7.8 ppm for the vacuum dried sample to -6.8 ppm at 43% RH and -6.1 ppm at 100% RH. It increases in intensity at 43% RH and decreases at 100% RH (Table 1). In contrast, for Na-hectorite this resonance is not observable at 100% RH, and although it is present at 43% RH, it's intensity is so low that it cannot be well characterized.

Likewise, the IR data show the intensities of the bands for symmetric and asymmetric CH_4 decrease with increasing RH and H_2O/cation ratio, with the intensity of the 2900 cm^{-1} peak decreasing more rapidly (Figure 7). The intensity of the 2900 cm^{-1} band for the Ca- and Pb-hectorites is much greater than for the Cs- and Na-hectorites, and it reaches a low, plateau value for the Ca- and Pb-samples at much larger H_2O/cation ratios.

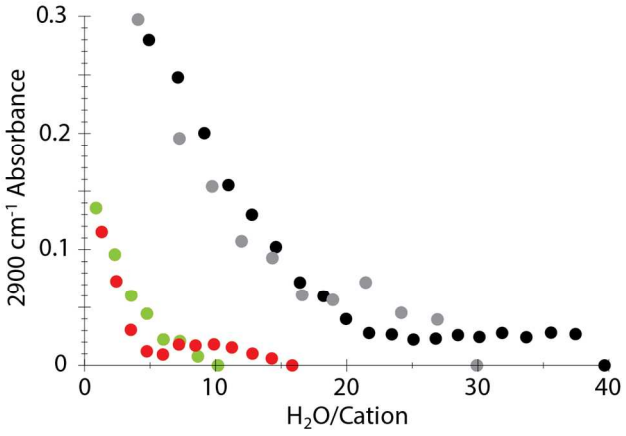

Figure 7. Intensity of the 2900 cm^{-1} ATR-IR band versus the H_2O/cation determined from the transmission IR data. The color coding is the same as in Figure 4; red – Na^+, green – Cs^+, grey – Pb^{2+}, black – Ca^{2+}. Note that there is a clear separation between the alkali metal and the divalent cation hectorites within the limits of uncertainty, but that overall, the absorption of the ν_1 band associated decreases in intensity as the H_2O content increases, in agreement with the NMR results for hectorite associated CH_4. The uncertainty on all data points is ±0.0025 absorbance units. The same data plotted versus the absolute H_2O uptake in mmol H_2O/g clay are available as Figure S4 in the Supporting Information.

DISCUSSION

Methane Adsorption Environments

The IR and NMR data both show that under our experimental conditions CH_4 occurs in the interlayer galleries of hectorite and in larger external pores. Signal in the ATR-IR spectra comes only from CH_4 associated with the clay, either on external particle surfaces or in the interlayer galleries. The observation of the normal P-Q-R branches of the asymmetric stretching band and the symmetry forbidden ν_1 band suggest that clay-associated CH_4 occurs in environments in which its electronic structure is not distorted (retains tetrahedral symmetry) and in which it is distorted from tetrahedral symmetry. Yamazaki et al. report the same symmetry forbidden ν_1 band for CH_4 adsorbed in the ~5 Å nano-pores of ZSM-5 zeolite,[49] and Wu et al. report it for CH_4 in silica.[50] Yamazaki et al. observe a change in frequency of this band with different charge balancing cations in ZSM-5, and interpret this variability as evidence that CH_4-cation interactions are responsible for the decrease in symmetry rather than simply adsorption in the pores.[49] Recent *ab initio* molecular dynamics (AIMD) calculations of CH_4 interactions with a Ca-montmorillonite[17] show that surface-associated CH_4 has dipole moments ranging from 0.25 to 1 Debye depending on the basal spacing and composition of the fluid, and also report strong interactions of this asymmetric CH_4 with the exchangeable cations. In contrast, in the spectra of our hectorites, the frequency of the ν_1 band is independent of the cation, in contrast to the

Yamazaki ZSM-5 results, leading us to conclude that interaction with the smectite layers themselves must be a significant contributor to the decreased symmetry of the CH_4 in these samples. The AIMD results of Lee et al. also show that asymmetric methane is frequently observed associated with OH groups on the smectite surface.[17] Thus, interaction with the surface or surface-adsorbed cations at any clay adsorption site (e.g., external basal surface, external layer edges, interlayer) could be responsible for the decreased CH_4 symmetry, and it is not possible to distinguish between different possible sorption sites using the ATR-IR spectra alone, particularly since the CH_4 producing the ν_1 site will also contribute intensity in the normal P-Q-R region. The decrease in the intensities of all the ATR-IR bands with increasing RH for all the samples clearly demonstrates progressive displacement of adsorbed CH_4 by H_2O, in agreement with the increased H_2O contents of the clay shown by the transmission IR data. This result is in agreement with the computational modeling results of Liu et al.[6] and Rao et al.[10-11] and also with the common assumption that water displaces hydrocarbons from the surfaces of silicate minerals. Our results also show that the H_2O uptake is greater with $scCH_4$ than with $scCO_2$ at 90 bar and 323 K, suggesting weaker interactions of the clays with CH_4 than with CO_2.[27]

The ^{13}C NMR results (Figures 4-6) add significantly to the understanding of IR data and show the presence of CH_4 in large pores between clay particles experiencing transient interactions with the external particle surfaces, in clay interlayers, and a minor amount of CH_4 in the bulk supercritical fluid state. Previous ^{13}C NMR studies of bulk $scCH_4$ and CH_4 in nano- and meso-porous materials show that confinement causes decreased shielding (less negative chemical shifts), with the size of this effect increasing with decreasing pore size.[19, 22-24, 26] This effect parallels that of the more extensively studied effects of pore size and substrate composition on the chemical shift of ^{129}Xe.[25, 51-52] Of particular interest are the spectra for $AlPO_4$-11[22] which, like

those reported here, contain three resonances and provide a basis for interpretation of our results. For $AlPO_4$-11, there is a narrow resonance representing the bulk gas phase, which Koskela et al.[22] use as the chemical shift reference. There is a resonance shifted ~ 4 ppm to less shielded values that they assign to CH_4 adsorbed in the nano-pores, for which the chemical shift change is not significantly dependent on temperature in the 230 – 380 K range. There is also a resonance with a chemical shift between these two that they assign to CH_4 in the large pores between the individual particles. The chemical shift of this resonance moves from near the value for CH_4 in the nano-pores at 230 K to within about 1.3 ppm of that of the bulk gas at 380 K. The authors evaluate this variability in peak position in terms of a 2-site exchange model, which has also been used to explain the observed chemical shifts of ^{129}Xe interacting with the external surfaces of mesoporous silica.[25] For a more extensive discussion of the ability to probe pore structure and exchange dynamics in porous silicas and silicates using ^{129}Xe and $^{13}CH_4$ interactions with porous silicas and silicates, see the Supporting Information.

As suggested above, the resonances for $^{13}CH_4$ in nano- and meso-porous materials can be greatly affected by site exchange processes,[22-23] and thus a brief discussion of two-site exchange is necessary before final assignment of the ^{13}C resonances observed for our samples. In a simple two-site exchange model, for separate resonances to be observed the frequency of exchange between sites must be smaller than approximately an order of magnitude less than the difference between the peak positions in frequency units. For the hectorites in this study, if exchange were occurring between the $^{13}CH_4$ environments represented by the resonances at -6.0 ppm and -10.0 to -10.4 ppm, separately observable peaks would require that the exchange frequency be less than approximately 50 Hz. In contrast, observation of a single, fully averaged peak for the exchanging sites requires exchange at frequencies greater than approximately 5 kHz. Here, rapid

exchange between resonances 4 ppm apart requires an exchange frequency greater than approximately 5,000 Hz. Rapid exchange is expected, for instance, among different, individual interlayer gallery sites, analogous to the behavior of H_2O and CO_2 molecules.[53-56] It is also expected between external surface sites and bulk $scCH_4$ in pores between clay particles, as discussed by Ok et al.[18] But rapid exchange may not occur for CH_4 in nano-confinement within the smectite interlayers and that in the external pores. The Supporting Information presents a more detailed discussion of the ability to probe structure and exchange dynamics in porous silicas and silicates using ^{129}Xe and $^{13}CH_4$.

Based on the IR and XRD results and the existing literature for related porous silicate materials discussed above and in the Supporting Information, we make the following assignments for the ^{13}C resonances in our hectorite samples. The small, very narrow (FWHH <0.05 ppm) peak at -10.3 ± 0.1 ppm is due to CH_4 in the bulk supercritical fluid phase that does not experience interactions with the hectorite particles on the NMR timescale. The chemical shift and line width are in good agreement with those of Ok et al.[18] This CH_4 may be in any large void space, such as in an underfilled rotor. The peaks between -6.0 and -8.2 ppm are due to CH_4 in the interlayer galleries of the hectorite, analogous to the CH_4 in the nano-pores of the methane hydrates[21, 24, 26] and molecular sieves.[22-23] The broad peak between -10.0 and -10.3 ppm is due to CH_4 in the larger pores between the individual hectorite particles, analogous to the resonances observed for CH_4 in the molecular sieves[22-23] and the ~4 nm pores in mesoporous silica.[19] The frequency of CH_4 exchange between interlayer sites and those of CH_4 in the external pores must be less than ~50 Hz since separate resonances are observed.

The changes in the ^{13}C spectra during accidental loss of CH_4 from the NMR rotor support the interpretation that the relatively broad peaks between -6.0 and -8.2 ppm represent interlayer CH_4

and those from -10.0 to -10.3 represent CH_4 in inter-particle pores (Figure 8). The spectrum of a vacuum dried Pb-hectorite that leaked CH_4 catastrophically contains a resonance at -6.8 ppm for interlayer CH_4 and one at -10.7 ppm for inter-particle CH_4, but no signal for bulk CH_4. The preferential retention of the interlayer and inter-particle CH_4 is as expected from the <50 Hz exchange frequency of CH_4 molecules between the bulk fluid and these environments. The ratio of interlayer CH_4/inter-particle CH_4 ratio for this sample is 0.52, substantially greater than the value of 0.35 for the fully pressurized sample, indicating that interlayer CH_4 is preferentially retained under these conditions. The chemical shift of -10.7 ppm for the inter-particle CH_4 is more negative than for the fully pressurized samples, as expected when the total fluid pressure in the sample is reduced, as shown in the variable pressure results of Ok et al.[18] The spectra of vacuum dried Cs-hectorite with a slow leak from the rotor acquired at 3 hrs, 3 hrs 10 min, and 5 hrs 15 min after charging also show preferential loss of inter-particle CH_4 (Figure 8). The intensities of the resonances for interlayer and inter-particle CH_4 at -7.8 to -7.9 ppm and -10.0 to -10.1 ppm remain constant at 10-11% and 88-89%, respectively, but that for bulk CH_4 at -10.5 to -10.7 pm decreases from ~ 1% to < 0.5%.

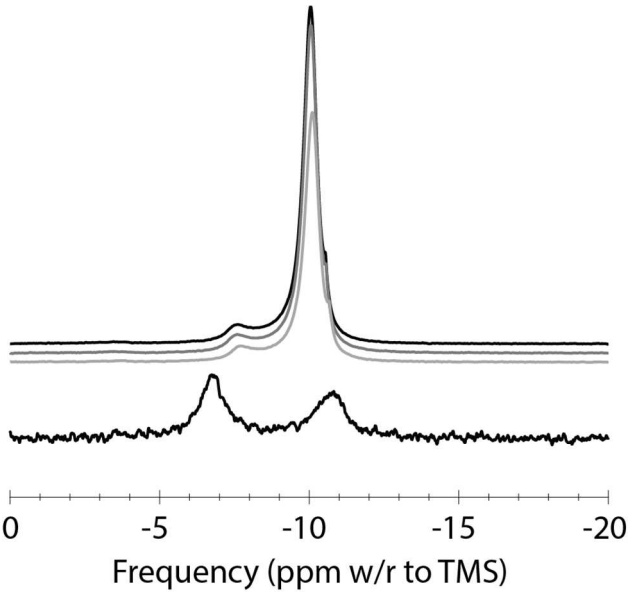

Figure 8. ^{13}C MAS NMR spectra (^{1}H decoupled) samples for which CH_4 accidentally leaked during data acquisition. The top three spectra are for vacuum dried Cs-hectorite with a slow leak from the rotor acquired at 3 hrs, 3 hrs 10 min, and 5 hrs 15 min after charging and are plotted at the correct relative intensity. The bottom spectrum is for vacuum dried Pb-hectorite after the $scCH_4$ leaked catastrophically. See text for discussion.

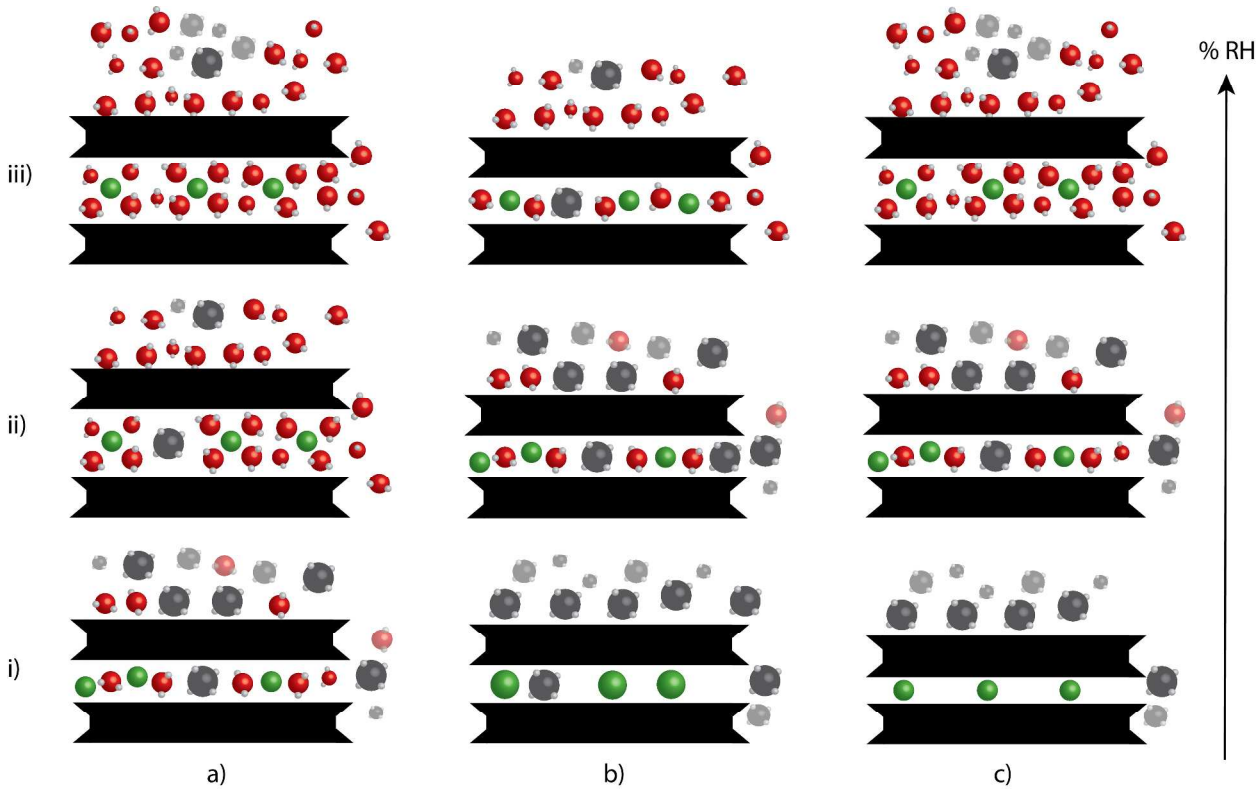

The relatively negative chemical shift for the bulk CH_4 is again consistent with decreased fluid pressure.[18]

Evolution of Interlayer CH_4 Environments with the H_2O Chemical Potential

The variation of the interlayer CH_4 ^{13}C chemical shift with the H_2O chemical potential (expressed as the RH of the $scCH_4$) can be readily understood based on the variation in the hectorite basal spacings obtained from the XRD data, the water contents obtained from the transmission IR data, and the idea suggested by Ok et al.[19] that the ^{13}C chemical shift becomes more negative with increasing average pore size (Figure 9). For the vacuum dried Ca- and Pb-hectorites, the resonances at -6.0 ppm are due to CH_4 in 1WL-type interlayers propped open by the water

Figure 9. Cartoon of the various CH_4 adsorption environments and how they and the basal spacing evolves with the chemical potential of H_2O in the scCH_4. The behavior of Ca^{2+} and Pb^{2+} hectorite is described in series (a), the behavior of Cs^+ hectorite in (b), and the behavior of Na^+ hectorite in (c). See detailed discussion in the main text.

molecules that IR shows are not removed by vacuum drying (Figures 1, 2, 9ai). With increasing RH, the chemical shifts of these resonances become more negative, and their relative intensities decrease (Table 1). The chemical shift change indicates an increase in the size of the average interlayer site occupied by CH_4, consistent with the increased average basal spacing from a 1WL-type to a 2WL-type interlayer fluid structure (a change in interlayer thickness from ~ 3.1 Å to ~7.4 Å based on the XRD basal reflections; Figures 2 and 9aii). The larger breadth of the interlayer CH_4 peaks relative to the bulk supercritical fluid may be due to a number of factors including exchange lifetime (T_2) broadening, chemical shift dispersion due to a distribution of adsorption site sizes/geometries, and distortion from T_d symmetry leading to a chemical shift anisotropy.[22-23] The relatively broad basal reflections observed by XRD suggest that a range of basal spacings are present, leading to a range of interlayer thicknesses and adsorption site dimensions that most certainly broaden the resonances due to chemical shift dispersion. The decrease in the relative intensity of the interlayer CH_4 resonance with increasing RH and basal spacing is consistent with a decreasing preference of the interlayers for CH_4 relative to H_2O shown in the IR data (Figure 9aiii). An increase in interlayer H_2O without a significant change in the basal spacing also explains the shift to more positive resonance frequency for interlayer CH_4 in Pb-hectorite from 43% RH to 100% RH (Table 1), since a larger interlayer H_2O content reduces the average volume probed by the CH_4 molecules. The decreased intensity of the resonances for interlayer CH_4 is also consistent with the relatively high hydration energies of these ions[46], and the low mutual solubilities of H_2O in CH_4 and CH_4 in H_2O,[33] suggesting that hydrated interlayers should prevent CH_4 intercalation. Interaction of the interlayer CH_4 with the

structural F^- at the base of the ditrigonal cavity appears to be quite weak. ^{19}F MAS NMR spectra of the vacuum dried Ca- hectorite sample shows essentially no change in the ^{19}F chemical shift of the two structurally different F-sites (Figure S5).

For the vacuum dried Cs-hectorite (Figure 9b), the -7.6 ppm chemical shift of the interlayer $^{13}CH_4$ resonance indicates a larger average CH_4 site than for interlayer CH_4 in the Ca- and Pb-samples at all conditions, consistent with the low H_2O content shown by the transmission IR data. The 11.2 Å basal spacing for vacuum dried Cs-hectorite results in an ~ 3.6 Å thick interlayer gallery, which may be just large enough to allow CH_4 molecules, which have a diameter of ~3.9 Å,[57] to enter (Figure 9bi). It is also possible that the CH_4 giving rise to this site may be dominantly in slightly expanded interlayers containing some H_2O molecules, as suggested by the transmission IR data. In either case, the relative absence of interlayer H_2O shown in the IR data for the vacuum-dried sample suggests that interlayer CH_4 unrestricted by the presence of H_2O can probe a larger pore volume on average. The progressively less negative chemical shifts for this resonance with

increasing RH (Table 1) indicates a progressively smaller interlayer CH_4 adsorption site despite the small increase in basal spacing. However, the transmission IR data indicate an increase in the interlayer H_2O, which likely reduces the lateral dimension parallel to the basal surface probed by the average interlayer CH_4 molecule (Figure 9bii). It is known that Cs smectites do not typically expand beyond a 1WL-type basal spacing,[27, 47] and the XRD results here show that it does not do so in contact with $scCH_4$ at 90 bar and 323 K even when the clay is pre-equilibrated at 100% RH. The increased relative intensity of this resonance for the 43% RH sample suggests that the ~1.0 Å increase in average basal spacing increases the fraction of interlayers in which CH_4 can intercalate. The decrease in intensity at 100% RH is, then, due to displacement of the

CH_4 by H_2O and the shift to more positive frequency indicates restriction of the interlayer CH_4 to probing an even smaller pore due to the presence of H_2O (Figure 9biii). For Na-hectorite, the 9.8 Å basal spacing of the fully dried sample results in an interlayer thickness of 2.2 Å, which is too small to allow entry of CH_4 in the interlayer galleries (Figure 9ci). Thus, the signal at -8.2 ppm observed for the vacuum dried sample is probably due to CH_4 in the small number of expanded interlayers (Figure 9cii) suggested by the XRD data and the small but detectable H_2O content in the transmission IR data. As for the Cs-hectorite, the addition of H_2O at 43% RH leads to a small shift to a more positive frequency indicating a slightly smaller average cage size due to the additional interlayer H_2O reducing the lateral volume probed by the intercalated CH_4 parallel to the clay surface (Figure 6; Table 1). The very small signal for this site for the 43% RH sample and its absence for the 100% RH sample (Table 1) indicates a strong preference of Na-hectorite interlayers for H_2O relative to CH_4 (Figure 9cii and 9ciii).

While the trends in our ^{13}C NMR data with increasing RH are consistent with expected trends in the mean pore size explored by intercalated CH_4, it is not possible to quantitatively determine the average pore size occupied by interlayer CH_4 from these data. This is because the ^{13}C NMR resonance frequency may depend on many factors, including the cation present, CH_4 dynamics, and the number of near neighbor H_2O and CH_4 molecules. Diffraction methods do not help in this regard, because they do not resolve specific interlayer sites. The cage diameters for the methane clathrates[21, 24, 26] and molecular sieves,[22-23] which yield resonances in the same chemical shift range, are typically in the 0.5 – 0.6 nm range, consistent with the thicknesses of the interlayer galleries for 1WL-type and 2WL-type structures. Computational molecular modeling will be helpful in providing more specific structural information for the clay interlayers, including the CH_4 adsorption site sizes, and the effect of their H_2O content on interlayer CH_4.

Surface Interactions and Evolution of Inter-particle Pore CH_4 with the H_2O Chemical Potential

The resonance for CH_4 in relatively large inter-particle pores is displaced from that for bulk $scCH_4$ at -10.3 ± 0.1 ppm by at most ~ 0.3 ppm and often merges with that of bulk CH_4 at higher RHs (Figures 4 and 6, Table 1). At all RHs, however, the increased peak width relative to that of bulk $scCH_4$ demonstrates that the inter-particle CH_4 is associated with the particle surfaces. The largest chemical shift displacement is less than the ~0.6 ppm displacement observed by Ok et al.[18] for CH_4 in ~ 4 nm pores of their amorphous silicas. Thus, it is likely that the average inter-particle pore dimension probed by CH_4 here is larger than this. We do not know the detailed microstructure of the clay packed in the NMR rotors spinning at ~ 10 kHz, but it is likely that the inter-particle pores are slit-like due to stacking of the clay layers (see Gilbert et al.[58] and references therein). Individual hectorite particles typically have lateral dimensions of the order of microns, and the CH_4 molecules are likely able to diffuse over that length on the millisecond time scale required for the observation of site averaging in our experiments. The position of this resonance at a given fluid pressure reflects the partitioning of CH_4 between sorption sites on the particle surfaces and in the interior of the pore, with the density of the fluid possibly being greater near the hectorite surface.[18] For a simple 2-site exchange model this chemical shift is given by the relationship $\delta_{obs} = a\delta_1 + b\delta_2$, where a is the fraction of the CH_4 in the pore adsorbed on the surface, δ_1 is the chemical shift of the surface sorbed CH_4, b is the fraction of the CH_4 in the pore not sorbed on the surface, and δ_2 is the average chemical shift of the CH_4 that is not surface sorbed. In this model with all else being equal (e.g., T, P, a, b, δ_1, and δ_2), the observed chemical shift depends on the surface area/volume ratio of the pore. Lifetime broadening (T_2) effects and distortion from T_d symmetry may contribute to the increased breadth of this peak relative to bulk $scCH_4$ (Table 1), but as for the interlayer sites, heterogeneity in the size of the

inter-particle pores is likely to contribute also by inducing chemical shift dispersion. For smectite clay samples, the slit-like external pores have much larger surface area/volume ratios than spherical or more equant pores, suggesting that a larger fraction of the CH_4 molecules in them could be interacting with the clay surface.

The general decrease in displacement, width and relative intensity of the inter-particle CH_4 peak with increasing RH for all the samples reflects the effects of increasing H_2O content. With increasing RH, the pores will progressively fill with H_2O, with the small pores and particle intersections filling first. This will reduce the inter-particle pore volume occupied by CH_4, resulting in the deceased intensity. Because the small pores fill first, the average size of the pores containing CH_4 will increase with increasing RH, consistent with the more negative chemical shift for inter-particle CH_4 with increasing RH. Likewise, the pore size distribution will decrease, leading to the observed decreased line widths. It is also possible that the fraction of CH_4 adsorbed on the external surfaces (the parameter *a* above) decreases, shifting the resonance closer to the position of bulk $scCH_4$, or that their ^{13}C chemical shift (δ_1 above) changes with increasing RH due to increased CH_4 interaction with adsorbed H_2O. Again, computational molecular modeling will be necessary to provide greater insight into the specific mechanisms responsible for the observed changes and their relative importance.

Thermodynamics of CH_4/Hectorite Interactions

Together, the results presented in this paper suggest that CH_4 adsorption in smectite interlayers is driven principally by weak dispersive interactions, with dipole interactions between asymmetric CH_4 molecules and H_2O molecules and the oxygen atoms of the smectite surface perhaps playing a role. This conclusion is in agreement with the results of computational GCMC modeling in the literature suggesting that CH_4/smectite interactions occur via a hydrophobic

mechanism,[16] recent AIMD modeling of $CH_4/CO_2/H_2O$ fluid interactions with Ca-montmorillonite that report dipole moments for CH_4 associated with cations or surfaces,[17] and the observed reduced symmetry of interlayer adsorbed CH_4 molecules shown in the IR results of this paper. This conclusion applies to intercalated CH_4 and that adsorption on external surfaces, although the following discussion is framed from the perspective of understanding CH_4 intercalation. As we recently discussed,[27] the equilibrium state of a clay interlayer in the presence of H_2O is governed by a balance among the free energies of hydration of the basal surfaces and the interlayer cations; electrostatic forces between the smectite T-O-T layers, ions, and H_2O dipoles; H_2O-H_2O and H_2O-clay surface hydrogen bonding interactions; weak dispersion interactions between all components; and any other fluid-surface, fluid-ion, and fluid-H_2O interactions in the system. For smectites in contact with a CH_4-rich fluid, the data here show that the interlayer must be propped open for CH_4 to enter it. Under our experimental conditions we never observe CH_4 inducing significant interlayer expansion, suggesting that interlayer propping occurs by H_2O intercalation. However, CH_4 intercalation is also feasible for hectorite in contact with CO_2/CH_4 fluids if CO_2 props open the interlayer, or in synthetic pillared clays in which the interlayers are propped open by precipitates. CH_4 cannot participate in hydrogen bonding networks and is charge neutral, both of which tend to make its adsorption and intercalation in smectites thermodynamically unfavorable with respect to H_2O adsorption. The absence of any effect of intercalated CH_4 on the ^{19}F NMR chemical shifts of the structural F^- of the hectorite (Figure S5) further supports this conclusion. However, the IR data suggest that interlayer adsorbed CH_4 does adopt an asymmetric structure that is expected to have a dipole moment, potentially increasing the favorability of its adsorption, as predicted in the molecular model of Lee et al.[17]

Based on these arguments, CH_4 must be incorporated into smectite interlayers primarily via a passive, space-filling mechanism. The RH dependences of the basal spacings determined by XRD resemble the hydration of smectites in the absence of CH_4 and do not indicate any significant expansion as a result of exposure to $scCH_4$ (Figure 2). Instead, interlayer CH_4 is only observed when the smectite is already expanded enough to accommodate it (basal spacing of ~11.5 Å) as a result of the adsorption of a sub-monolayer of H_2O on average. The XRD results for Cs-hectorite here are particularly helpful in identifying the passive role of CH_4 in smectite expansion. The statistically insignificant change in its basal spacing when exposed to dry $scCH_4$ contrasts with the ~1 Å expansion in contact with dry $scCO_2$ caused by CO_2 intercalation.[27] Thus, CO_2 seems to play an active role in expanding Cs-hectorite, whereas CH_4 passively enters the interlayer without providing an energetic driver to induce significant expansion.

CONCLUSIONS

^{13}C MAS NMR spectroscopy, IR spectroscopy, and X-ray diffraction results for the smectite mineral hectorite at 90 bar CH_4 pressure and 323 K show that CH_4 occurs in interlayer sites, in inter-particle pores, and in bulk $scCH_4$ fluid not interacting significantly with the clay. The RH of the $scCH_4$ phase and the hydration energy and size of the charge-balancing cation of CH_4 greatly affect the CH_4 partitioning among these environments. These data are the first *in situ* spectroscopic evidence of interlayer CH_4 adsorption in smectite interlayers at petroleum reservoir conditions, and show that for this to occur the thermodynamic activity of water (RH) in the reservoir must be appropriate for 1WL- or 2WL-type interlayers to form, depending on the charge balancing cation. CH_4 can intercalate the interlayer only at basal spacings above a critical threshold of ~11.5 Å, and the amount of interlayer adsorption is greatest at low H_2O contents when there are many interlayer adsorption sites unoccupied by cations or H_2O and when the

number of charge-balancing cations in the interlayer is relatively low (e.g., Ca^{2+} and Pb^{2+} vs. Cs^{+} and Na^{+}). The results indicate that CH_4 adsorbs to smectite interlayers principally by a weak hydrophobic mechanism dominated by dispersion-type forces, leading to a passive, space-filling model for its intercalation. The ATR-IR data shows that adsorption of CH_4 reduces its tetrahedral, T_d, symmetry. The results also show that CH_4 in our samples occurs in external pores between clay particles, with the NMR behavior of this CH_4 becoming more like that of bulk methane as the water content increases. These findings are in excellent agreement with previously published thermodynamic, molecular modeling, and gravimetric data.

One implication of our results is that CH_4 can be adsorbed in smectite interlayers at low H_2O conditions. Such conditions may be produced during a dry $scCO_2$ flood of an oil or gas reservoir or fracking of a tight reservoir using CO_2. CH_4 intercalation is greater with divalent interlayer cations (Ca^{2+} and Pb^{2+}) than with Na^{+}. This result suggests that ion exchange reactions occurring in shales as a result of fracking or natural gas extraction (e.g. dissolution of calcite due to interaction with wet $scCO_2$ that liberates Ca^{2+} that can exchange with the parent smectite charge balancing cation) may alter the extent of interaction between CH_4 and clays in the rocks. Whether the net effect is an increase or decrease in interlayer adsorbed CH_4 depends on the initial charge-balancing cation and the RH of the fluid phase. CH_4 intercalation is also quite large with interlayer Cs^{+}, suggesting that Cs-exchanged smectites may be effective materials for CH_4 sorption and separation. Since CH_4 adsorption is driven by a hydrophobic mechanism, more hydrophobic smectites, such as those containing significant quantities of fluorine, are likely to better sorb methane than smectites with greater hydrophilicity.

The results also highlight how integration of multiple *in situ* experimental methods can provide a richer picture of the molecular-scale of the interaction of mineral surfaces and supercritical

fluids than using one method alone. The results here will be an important reference to calibrate and validate the results of computational molecular modeling studies in the coming years.

As a final point, though there is excellent agreement between the IR, XRD, and NMR results in this study, we acknowledge that the centrifugal forces experienced during the NMR experiments present a potential source of variability between the IR, XRD, and NMR samples. Rapid rotation could conceivably influence the inter-particle pore shapes or volumes, accessibility to interlayer pores if it leads to preferential orientation of clay platelets, and perhaps even alter the partitioning of the fluids. We did not observe physical evidence of sample compression that is often observed at higher rotation rates at the 5 kHz spin rate used in these studies, which also makes it unlikely that rotation altered the clay platelet orientations in a fashion that limits access of CH_4 to interlayer pores. The small spinning sidebands observed in MAS NMR spectra of pure scCH_4 is evidence that the CH_4 can densify near the sample walls of an empty rotor; however, the sideband intensity is very small and thus we do not believe rotation in a tightly packed powder will influence the CH_4 partitioning. Ongoing studies in our group are assessing the influence that sample density plays on the results from all three instruments (XRD, IR, NMR).

AUTHOR CONTRIBUTIONS

The manuscript was written through contributions of all authors. All authors have given approval to the final version of the manuscript.

SUPPORTING INFORMATION – Discussion of the ^{19}F MAS NMR results and associated figure; comparison of the CH_4 asymmetric stretching region of the ATR-IR data; vacuum/dry

$scCH_4$ basal peak comparison from *in situ* XRD; table of masses/mole information for each NMR experiment

ACKNOWLEDGMENTS

The work in this manuscript was supported by the United States Department of Energy, Office of Science, Office of Basic Energy Science, Chemical science, Biosciences, and Geosciences division through their programs at MSU (DE-FG02-08ER15929, RJK, GMB, SSC, NL) and at Pacific Northwest National Laboratory (JSL). HTS was supported by the U.S. Department of Energy, Office of Fossil Energy. GMB was also supported through the United States Department of Energy, Office of Science, Office of Workforce Development for Teachers and Scientists Visiting Faculty Program and Pacific Northwest National Laboratory Associated Fellowship Program. SSC was supported through the United States Department of Energy, Office of Science, Office of Workforce Development for Teachers and Scientists Summer Undergraduate Laboratory Internship program. The NMR data in this work was collected via a Science Theme Proposal (ID: 48812 and 49782) using instrumentation at the Environmental Molecular Science Laboratory, a DOE Office of Science User Facility sponsored by the Office of Biological and Environmental Research and located at Pacific Northwest National Laboratory. PNNL is operated by Battelle for the DOE under Contract DE-AC05-76RL01830.

REFERENCES

1. Schnoor, J. L., Shale Gas and Hydrofracturing. *Environ. Sci. Technol.* **2012**, *46*, 4686-4686.
2. Agency, I. E. *Are We Entering a Golden Age of Gas?*; Paris, France, 2011.
3. Elliot, T. R.; Celia, M. A., Potential Restrictions for CO_2 Sequestration Sites Due to Shale and Tight Gas Production. *Environ Sci Technol* **2012**, *46*, 4223-4227.
4. Jackson, R. B.; Vengosh, A.; Carey, J. W.; Davies, R. J.; Darrah, T. H.; O'Sullivan, F.; Petron, G., The Environmental Costs and Benefits of Fracking. *An. Rev. Environ. Resources* **2014**, *39*, 327-362.

5. Ilgen, A. G.; Heath, J. E.; Akkutlu, I. Y.; Bryndzia, L. T.; Cole, D. R.; Kneafsey, T. J.; Milliken, K. L.; Pyrak-Nolte, L. J.; Suarez-Rivera, R., Shales at All Scales: Exploring Coupled Processes in Mudrocks. *Earth-Science Reviews* **2017**, *166*, 132-152.
6. Liu, D.; Yuan, P.; Liu, H.; Li, T.; Tan, D.; Yuan, W.; He, H., High Pressure Adsorption of Methane on Montmorillonite, Kaolinite, and Illite. *Appl. Clay Sci.* **2013**, *85*, 25-30.
7. Liang, L.; Xiong, J.; Liu, X.; Luo, D., An Investigation into the Thermodynamic Characteristics of Methane Adsorption on Different Clay Minerals. *J. Natural Gas Sci. Engin.* **2016**, *33*, 1046-1055.
8. Ji, L.; Zhang, T.; Milliken, K. L.; Qu, J.; Zhang, X., Experimental Investigation of Main Controls to Methane Adsorption in Clay-Rich Rocks. *Appl. Geochem.* **2012**, *27*, 2533-2545.
9. Ross, D. J. K.; Bustin, R. M., The Importance of Shale Composition and Pore Structure Upon Gas Storage Potential of Shale Gas Reservoirs. *Mar. Petrol. Geol.* **2009**, *26*, 916-927.
10. Rao, Q.; Xiang, Y.; Leng, Y., Molecular Simulations on the Structure and Dynamics of Water-Methane Fluids between Na-Montmorillonite Clay Surfaces at Elevated Temperature and Pressure. *J. Phys. Chem. C* **2013**, *117*, 14061-14069.
11. Rao, Q.; Leng, Y., Methane Aqueous Fluids in Montmorillonite Clay Interlayer under near-Surface Geological Conditions: A Grand Canonical Monte Carlo and Molecular Dynamics Simulation Study. *J. Phys. Chem. B* **2014**, *118*, 10956-10965.
12. Senna, M. M.; Morrow, C. P.; Kirkpatrick, R. J.; Krishnan, M., Structure, Energetics, and Dynamics of Supercritical Carbon Dioxide at Smectite Mineral-Water Interfaces: Molecular Dynamics Modeling and Adaptive Force Investigation of CO_2/H_2O Mixtures Nanoconfined in Na-Montmorillonite. *Chem. Mater.* **2015**, *27*, 6946-6959.
13. Zhang, H.; Cao, D., Molecular Simulation of Displacement of Shale Gas by Carbon Dioxide at Different Geological Depths. *Chem. Engin. Sci.* **2016**, *156*, 121-127.
14. Zhang, J.; Clennell, M. B.; Liu, K.; Pervukhina, M.; Chen, G.; Dewhurst, D. N., Methane and Carbon Dioxide Adsorption on Illite. *Energ. Fuel* **2016**, *30*, 10643-10652.
15. Gadikota, G.; Dazas, B.; Rother, G.; Cheshire, M. C.; Bourg, I. C., Hydrophobic Solvation of Gases (CO_2, CH_4, H_2, Noble Gases) in Clay Interlayer Nanopores. *J. Phys. Chem. C* **2017**, *121*, 26539-26550.
16. Jin, Z.; Firoozabadi, A., Methane and Carbon Dioxide Adsorption in Clay-Like Slit Pores by Monte Carlo Simulations. *Fluid Phase Equilib.* **2013**, *360*, 456-465.
17. Lee, M.-S.; McGrail, B. P.; Rousseau, R.; Glezakou, V. A., Molecular Level Investigation of CH_4 and CO_2 Adsorption in Hydrated Calcium Montmorillonite. *J. Phys. Chem. C* **2018**, *122*, 1125-1134.
18. Cole, D. R.; Ok, S.; Striolo, A.; Phan, A., Hydrocarbon Behavior at Nanoscale Interfaces. *Rev. Mineral. Geochem.* **2013**, *75*, 495-545.
19. Ok, S.; Hoyt, D. W.; Andersen, A. K.; Sheets, J.; Welch, S. A.; Cole, D. R.; Mueller, K. T.; Washton, N. M., Surface Interactions and Confinement of Methane: A High Pressure Magic Angle Spinning NMR and Computational Chemistry Study. *Langmuir* **2017**, *33*, 1359-1367.
20. Koh, D.-Y.; Kang, H.; Kim, D.-O.; Park, J.; Cha, M.; Lee, H., Recovery of Methane from Gas Hydrates Intercalated within Natural Sediments Using CO_2 and a CO_2/N_2 Gas Mixture. *Chem. Sustain. Chem.* **2012**, *5*, 1443-1448.
21. Yeon, S.-H.; Seol, J.; Seo, Y.-J.; Park, Y.; Koh, D.-Y.; Park, K.-P.; Huh, D.-G.; Lee, J.; Lee, H., Effect of Interlayer Ions on Methane Hydrate Formation in Clay Sediments. *J. Phys. Chem. B* **2009**, *115*, 1245-1248.

22. Koskela, R.; Ylihautala, M.; Jokisaari, J.; Vaara, J., C-13 NMR of Methane in an $AlPO_4$-11 Molecular Sieve: Exchange Effects and Shielding Anisotropy. *Phys. Rev. B* **1998**, *53*, 14833-14836.
23. Koskela, T.; Ylihautala, M.; Vaara, J.; Jokisaari, J., C-13 NMR of Methane Adsorbed in SAPO-11 Molecular Sieves. *Chem. Phys. Lett.* **1996**, *261*, 425-430.
24. Fleyfel, F.; Song, K. Y.; Kook, A.; Martin, R.; Kobayashi, R., Interpretation of C-13 NMR of Methane/Propane Hydrates in the Metastable/Nonequilbirum Region. *J. Phys. Chem.* **1993**, *97*, 6722-6725.
25. Terskikh, V. V.; Moudrakovski, I. L.; Breeze, S. R.; Lang, S.; Ratcliffe, C. I.; Ripmeester, J. A.; Sayari, A., A General Correlation for the Xe-129 NMR Chemical Shift-Pore Size Relationship in Porous Silica-Based Materials. *Langmuir* **2002**, *18*, 5653-5656.
26. Ripmeester, J. A.; Ratcliffe, C. I., Low Temperature Cross Polarization Magic Angle Spinning C-13 NMR of Solid Methane Hydrates: Structure, Cage Occupancy, and Hydration Number. *J. Phys. Chem.* **1988**, *92*, 333-339.
27. Bowers, G. M.; Schaef, H. T.; Loring, J. S.; Hoyt, D. W.; Burton, S. D.; Walter, E. D.; Kirkpatrick, R. J., Role of Cations in CO_2 Adsorption, Dynamics, and Hydration in Smectite Clays under in Situ Supercritical CO_2 Conditions. *J. Phys. Chem. C* **2017**, *121*, 577-592.
28. Loring, J. S.; Ilton, E. S.; Chen, J.; Thompson, C. J.; Martin, P. F.; Benezeth, P.; Rosso, K. M.; Felmy, A. R.; Schaef, H. T., In Situ Study of CO_2 and H_2O Partitioning between Na-Montmorillonite and Variably Wet Supercritical Carbon Dioxide. *Langmuir* **2014**, *30*, 6120-6128.
29. Loring, J. S., et al., In Situ Molecular Spectroscopic Evidence for CO_2 Intercalation into Montmorillonite in Supercritical Carbon Dioxide. *Langmuir* **2012**, *28*, 7125-7128.
30. Schaef, H. T., et al., Competitive Sorption of CO_2 and H_2O in 2:1 Layer Phyllosilicates. *Geochim. Cosmochim. Acta* **2015**, *161*, 248-257.
31. Ilton, E. S.; Schaef, H. T.; Qafoku, O.; Rosso, K. M.; Felmy, A., In Situ X-Ray Diffraction Study of Na^+ Saturated Montmorillonite Exposed to Variably Wet Supercritical CO_2. *Environ. Sci. Technol.* **2012**, *46*, 4241-4248.
32. Rother, G., et al., CO_2 Sorption to Subsingle Hydration Layer Montmorillonite Clay Studies by Excess Sorption and Neutron Diffraction Measurements. *Environ. Sci. Technol.* **2013**, *47*, 205-211.
33. Loring, J. S.; Bacon, D. H.; Springer, R. D.; Anderko, A.; Gopinath, S.; Yonkofski, C. M.; Thompson, C. J.; McGrail, B. P.; Rosso, K. M.; Schaef, H. T., Water Solubility at Saturation for CO_2-CH_4 Mixtures at 323.2 K and 9.000 Mpa. *J. Chem. Engin. Data* **2017**, *62*, 1608-1614.
34. Bowers, G. M.; Hoyt, D. W.; Burton, S. D.; Ferguson, B. O.; Varga, T.; Kirkpatrick, R. J., In Situ ^{13}C and ^{23}Na Magic Angle Spinning NMR Investigation of Supercritical CO_2 Incorporation in Smectite-Natural Organic Matter Composites. *J. Phys. Chem. C* **2014**, *118*, 3564-3573.
35. Dazas, B.; Lanson, B.; Breu, J.; Robert, J.-L.; Pelletier, M.; Ferrage, E., Smectite Fluorination and Its Impact on Interlayer Water Content and Structure: A Way to Fine Tune the Hydrophilicity of Clay Surfaces? *Micropor. Mesopor. Mat.* **2013**, *181*, 233-247.
36. Arroyo, L. J.; Li, H.; Teppen, B. J.; Boyd, S. A., A Simple Purification Method for Reference Clays. *Clays Clay Miner.* **2005**, *53*, 511-519.
37. Bowers, G. M.; Singer, J. W.; Bish, D. L.; Kirkpatrick, R. J., Alkali Metal and H_2O Dynamics at the Smectite/Water Interface. *J. Phys. Chem. C* **2011**, *115*, 23395-23407.

38. Bowers, G. M.; Singer, J. W.; Bish, D. L.; Kirkpatrick, R. J., Structural and Dynamical Relationships of Ca^{2+} and H_2O in Smectite/^2H_2O Systems. *Am. Mineral.* **2014**, *99*, 318-331.
39. Thompson, C. J.; Martin, P. F.; Chen, J.; Benezeth, P.; Schaef, H. T.; Rosso, K. M.; Felmy, A. R.; Loring, J. S., Automated High-Pressure Titration System with in Situ Infrared Spectroscopic Detection. *Rev. Sci. Instrum.* **2014**, *85*, 044102/1-044102/11, doi: 10.1063/1.4870411.
40. Miller, Q. R. S.; Thompson, C. J.; Loring, J. S.; Windisch, C. F.; Bowden, M. E.; Hoyt, D. W.; Hu, J. Z.; Arey, B. W.; Rosso, K. M.; Schaef, H. T., Insights into Silicate Carbonation Processes in Water-Bearing Supercritical CO_2 Fluids. *Internat. J. Greenhouse Gas Contr.* **2013**, *15*, 104-118.
41. Schaef, H. T.; Ilton, E. S.; Qafoku, O.; Martin, P. F.; Felmy, A.; Rosso, K. M., In Situ XRD Study of Ca^{2+} Saturated Montmorillonite (STx-1) Exposed to Anhydrous and Wet Supercritical Carbon Dioxide. *Internat. J. Greenhouse Gas Contr.* **2012**, *6*, 220-229.
42. Loring, J. S.; Thompson, C. J.; Wang, Z.; Joly, A. G.; Sklarew, D. S.; Schaef, H. T.; Ilton, E. S.; Rosso, K. M.; Felmy, A. R., In Situ Infrared Spectroscopic Study of Forsterite Carbonation in Wet Supercritical CO_2. *Environ. Sci. Technol.* **2011**, *45*, 6204-10.
43. Loring, J. S.; Thompson, C. J.; Zhang, C.; Wang, Z.; Schaef, H. T.; Rosso, K. M., In Situ Infrared Spectroscopic Study of Brucite Carbonation in Dry to Water-Saturated Supercritical Carbon Dioxide. *J. Phys. Chem. A* **2012**, *116*, 4768-77.
44. Walter, E. D.; Qi, L.; Chamas, A.; Mehta, H. S.; Sears, J. A.; Scott, S. L.; Hoyt, D. W., Operando MAS NMR Reaction Studies at High Temperatures and Pressures. *J. Phys. Chem. C* **2018**, *122*, 8209-8215.
45. Bowers, G. M.; Bish, D. L.; Kirkpatrick, R. J., H_2o and Cation Structure and Dynamics in Expandable Clays: ^2H and ^{39}K NMR Investigations of Hectorite. *J. Phys. Chem. C* **2008**, *112*, 6430-6438.
46. Smith, D. W., Ionic Hydration Enthalpies. *J. Chem. Educ.* **1977**, *54*, 540-542.
47. Berend, I.; Cases, J.; Francois, M.; Uriot, J. P.; Michot, L. J.; Masion, A.; Thomas, F., Mechanism of Adsorption and Desorption of Water Vapor by Homoionic Montmorillonites: 2. The Li+, Na+, K+, Rb+, and Cs+-Exchanged Forms. *Clays Clay Miner.* **1995**, *43*, 324-336.
48. Cases, J. M.; Berend, I.; Francois, M.; Uriot, J. P.; Michot, L. J.; Thomas, F., Mechanism of Adsorption and Desorption of Water Vapor by Homoionic Montmorillonite: 3. The Mg2+, Ca2+, Sr2+ and Ba2+ Exchanged Forms. *Clays Clay Miner.* **1997**, *45*, 8-22.
49. Yamazaki, T.; Watanuki, I.; Ozawa, S.; Ogino, Y., Infrared Spectra of Methane Adsorbed by Ion-Exchanged ZSM-5 Zeolites. *Langmuir* **1998**, *4*, 433-438.
50. Wu, J. L. S.; Li, G.; Li, C.; Li, C.; Xin, Q., FTIR Investigation of Methane Adsorption on Silica. *Appl. Surf. Sci.* **1994**, *81*, 37-41.
51. Janicke, M.; Chmelka, B. F.; Larsen, R. G.; Shore, J.; Schmidtrohr, K.; Emsley, L.; Long, H.; Pines, A., 2-Dimensional Xe-129 Exchange NMR Measurements of Xenon Dynamics in Na-A Zeolite. *Stud. Surf. Sci. Catal.* **1994**, *84*, 519-526.
52. Wernett, P. C.; Larsen, J. W.; Yamada, O.; Yue, H. J., Determination of the Average Micropore Diameter of an Illinois No-6-Coal by Xe-129 NMR. *Energ. Fuel* **1990**, *4*, 412-413.
53. Reddy, U. V.; Bowers, G. M.; Loganathan, N.; Bowden, M. E.; Yazaydin, A. O.; Kirkpatrick, R. J., Water Structure and Dynamics in Smectites:X-Ray Diffraction and ^2H-NMR Spectroscopy of Mg, Ca, Sr, Na, Cs, and Pb-Hectorite. *J. Phys. Chem. C* **2016**, *120*, 8863-8876.
54. Loganathan, N.; Yazaydin, A. O.; Bowers, G. M.; Kalinichev, A. G.; Kirkpatrick, R. J., Molecular Dynamics Study of CO_2 and H_2O Intercalation in Smectite Clays: Effect of

Temperature and Pressure on Interlayer Structure and Dynamics in Hectorite. *J. Phys. Chem. C* **2017**, *121*, 24527-24540.
55. Sena, M. M.; Morrow, C. P.; Kirkpatrick, R. J.; Krishnan, M., Supercritical Carbon Dioxide at Smectite Mineral-Water Interfaces: Molecular Dynamics and Adaptive Biasing Force Investigation of CO_2/H_2O Mixtures Nanoconfined in Na-Montmorillonite. *Chem. Mater.* **2015**, *27*, 6946-6959.
56. Morrow, C. P.; Yazaydin, A. O.; Kalinichev, A. G.; Bowers, G. M.; Kirkpatrick, R. J., Structure and Dynamics of Clay Surfaces and Interlayers: Molecular Dynamics Investigations of Na-Hectorite. *J. Phys. Chem. C* **2013**, *116*, 22987-22991.
57. Hirschfelder, J. O.; Curtiss, C. F.; Bird, R. B., *Molecular Theory of Gases and Liquids*; Wiley: New York, 1954.
58. Gilbert, B.; Comolli, L. R.; Tinnacher, R. M.; Kunz, M.; Banfield, J. F., Formation and Restacking of Disordered Smectite Osmotic Hydrates. *Clays Clay Miner.* **2015**, *63*, 432-442.

TOC Graphic

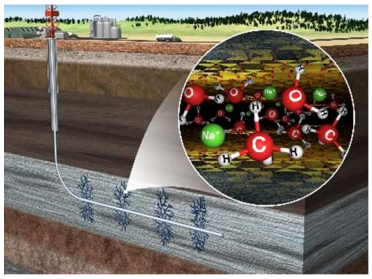

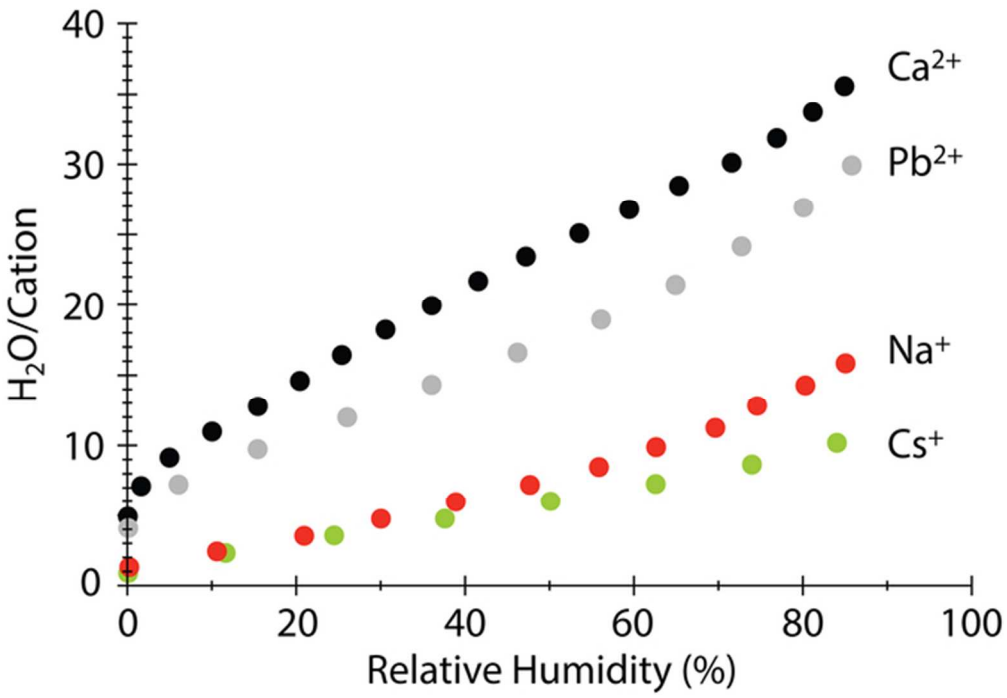

Figure 1

56x39mm (300 x 300 DPI)

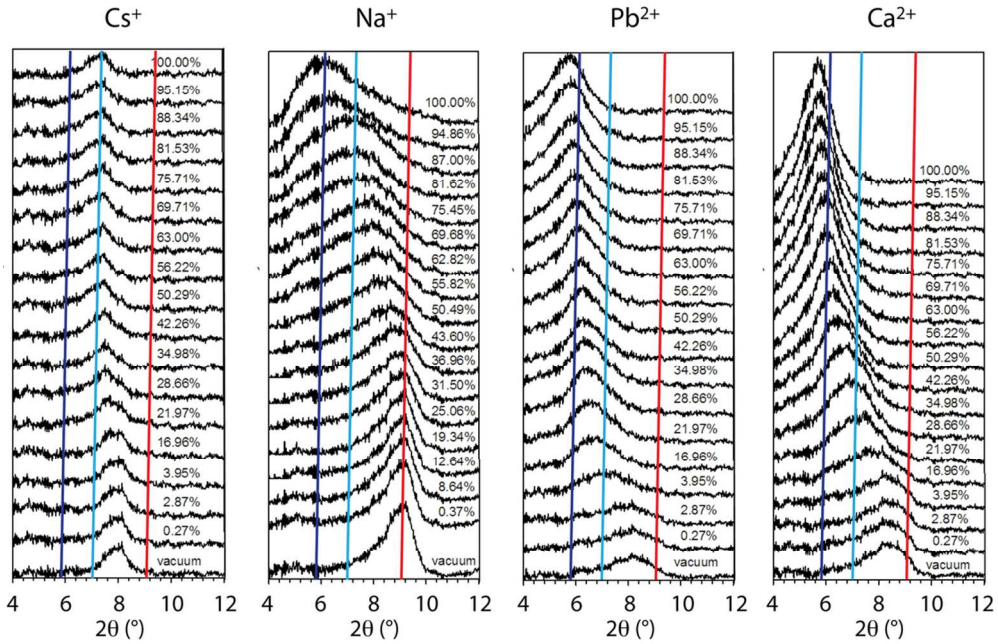

Figure 2

106x69mm (300 x 300 DPI)

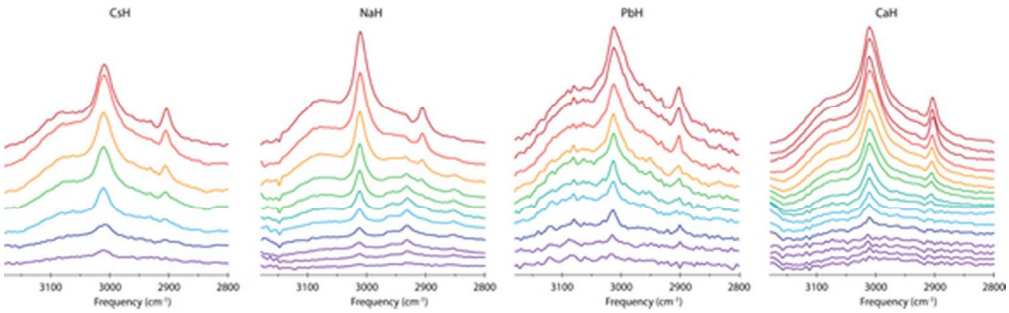

Figure 3

49x14mm (300 x 300 DPI)

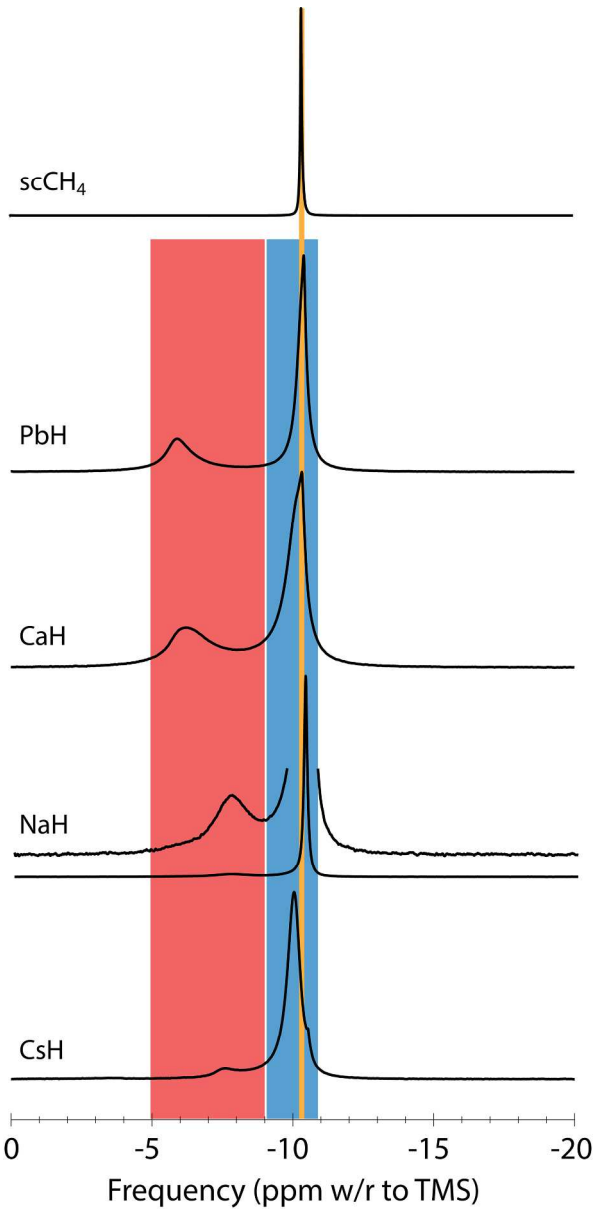

Figure 4

168x342mm (300 x 300 DPI)

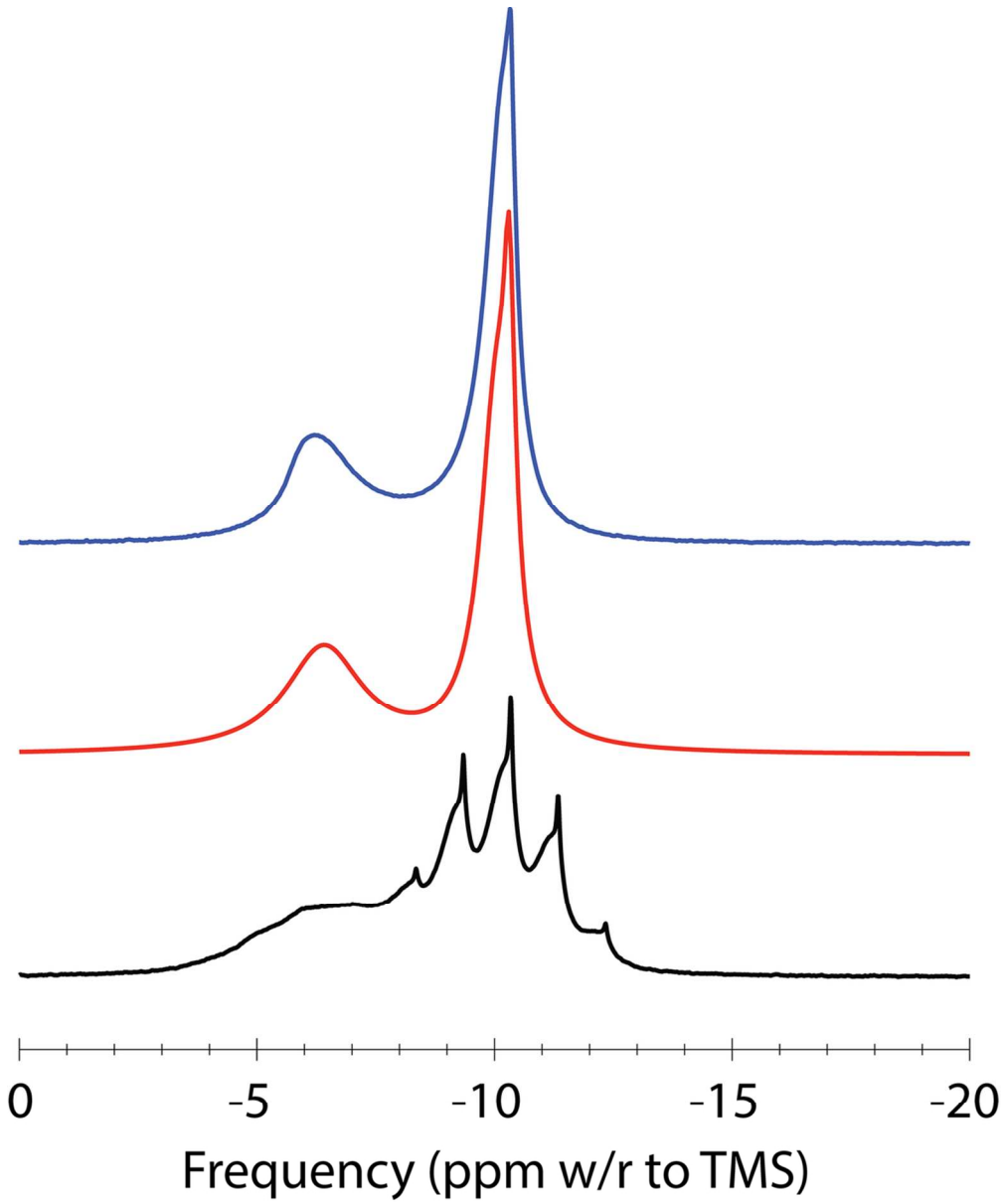

Figure 5

99x119mm (300 x 300 DPI)

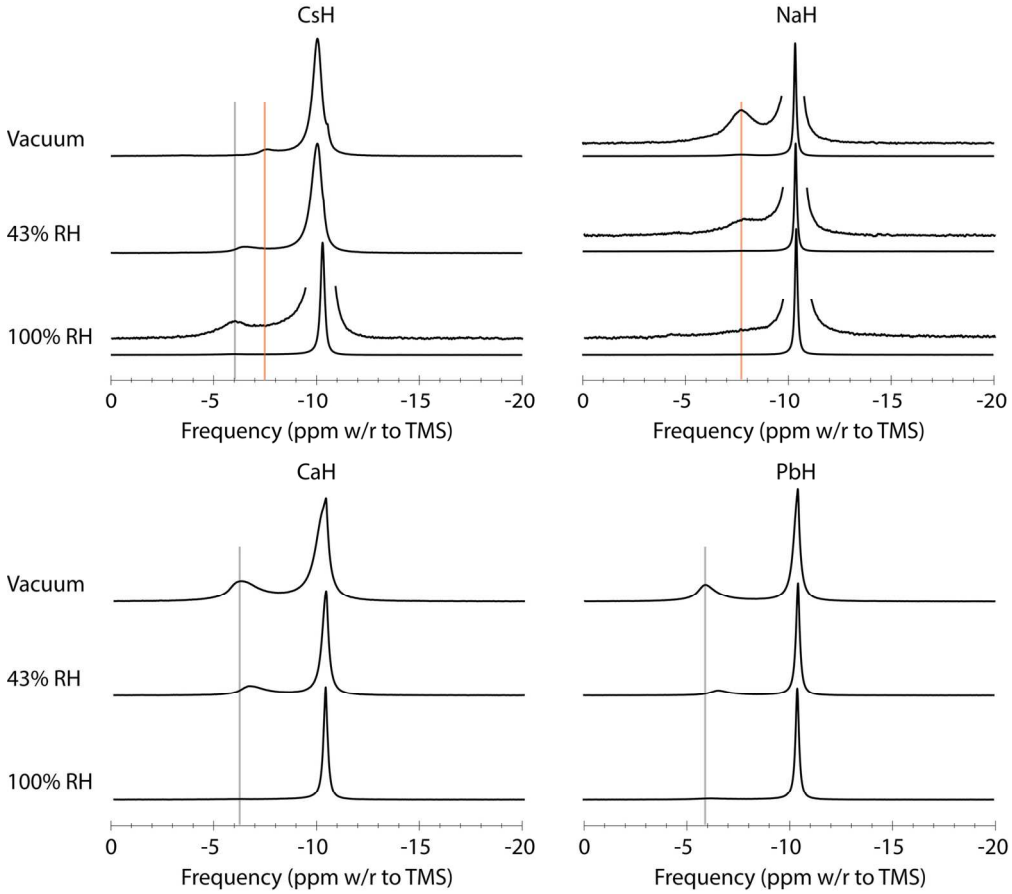

Figure 6

146x129mm (300 x 300 DPI)

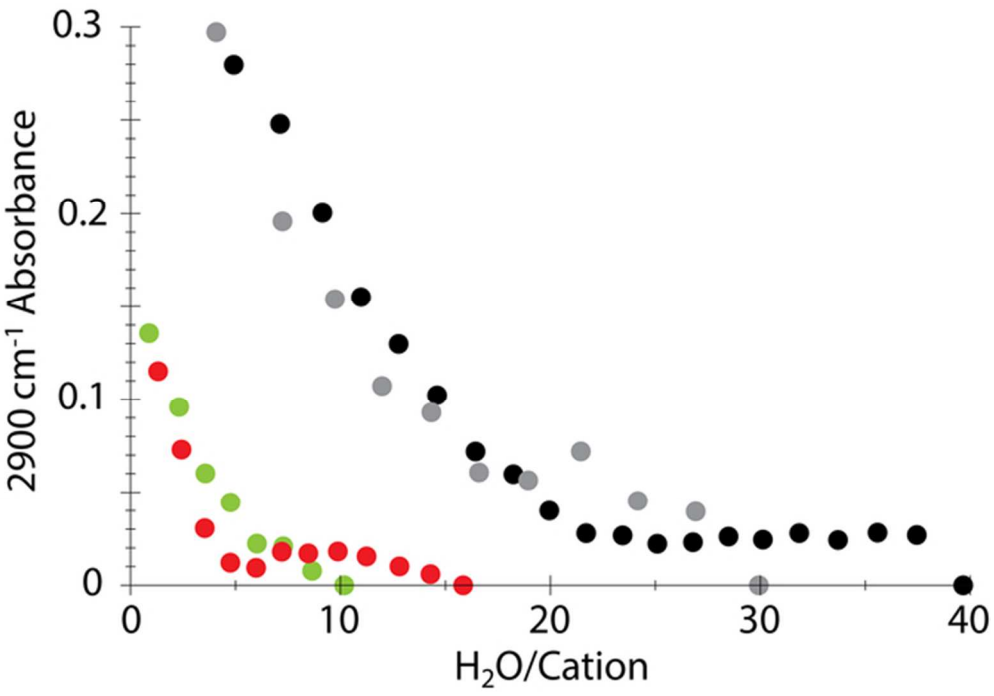

Figure 7

57x39mm (300 x 300 DPI)

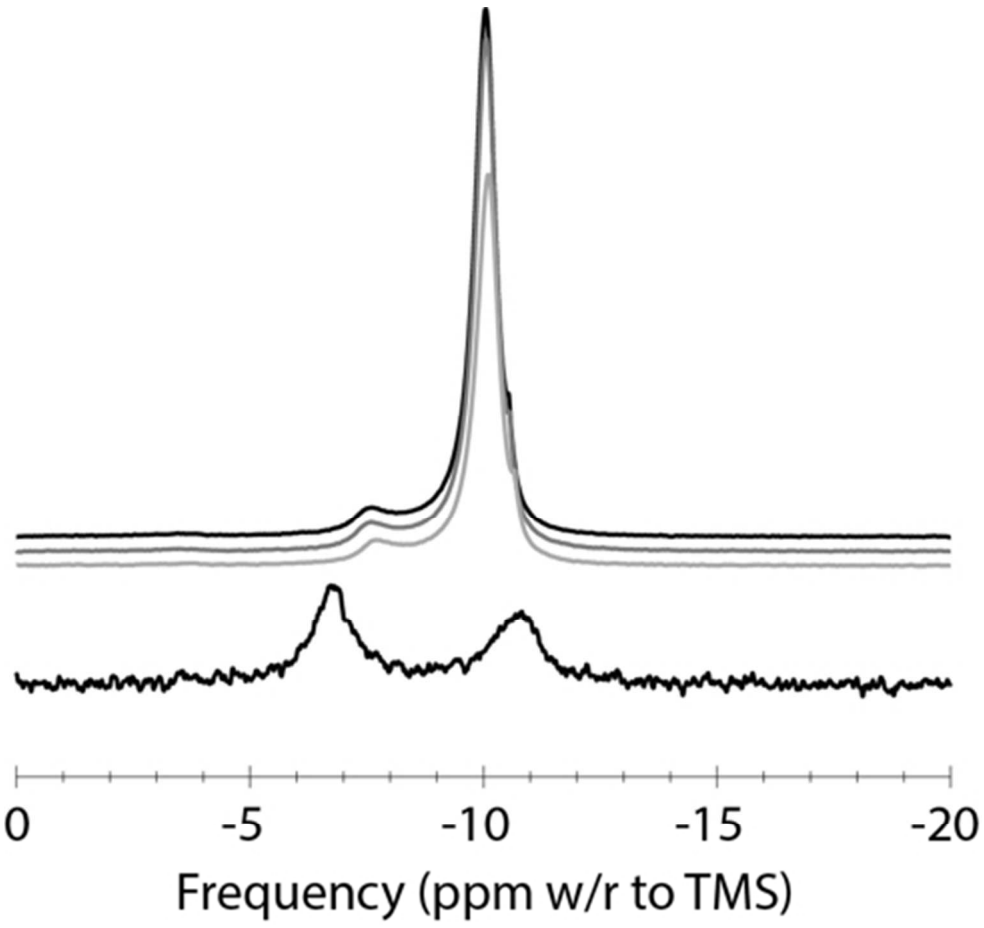

Figure 8

82x77mm (150 x 150 DPI)

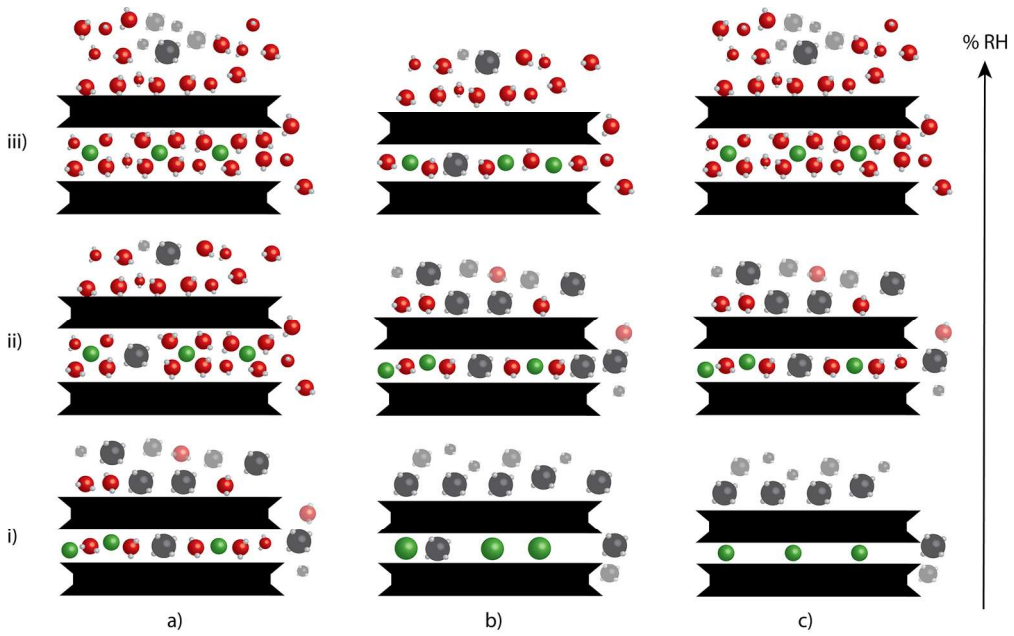

Figure 9

165x103mm (300 x 300 DPI)

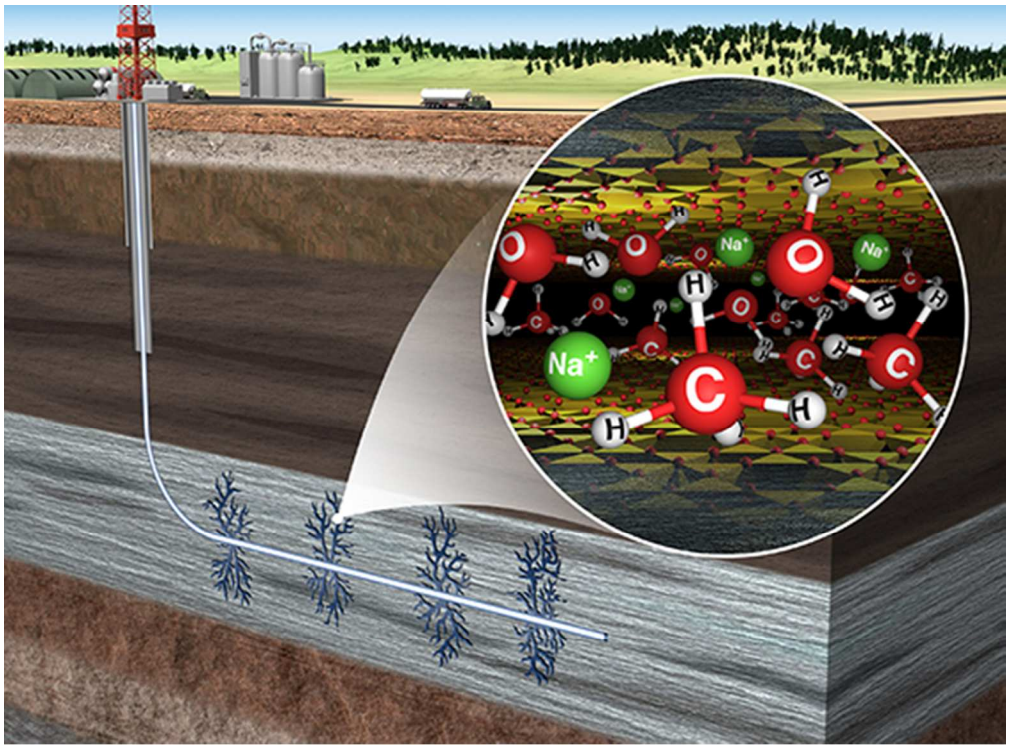

TOC Graphic

48x35mm (300 x 300 DPI)